PHYSICAL REVIEW B VOLUME 25, NUMBER 2 15 JANUARY 1982

Electron-energy-loss spectroscopy and ordered adsorbate layers on the Ni(100) surface

Talat S. Rahman, J. E. Black, and D. L. Mills
Department of Physics, University of California, Irvine, California 92717
(Received 18 May 1981)

We have studied the lattice dynamics of ordered overlayers of adsorbate atoms on the (100) surface of an fcc crystal, with emphasis on contact with recent electron-energy-loss data on the $p(2\times2)$ and $c(2\times2)$ overlayers of oxygen on the Ni(100) surface. This is done within a model that fits the bulk phonon spectrum of Ni with nearest-neighbor central-force couplings, and extracts adsorbate-substrate force constants from *ab initio* calculations of potential-energy curves carried out by Upton and Goddard. We obtain a very good fit to the data, but only if we assume the $c(2\times2)$ layer to be much closer to the surface than the $p(2\times2)$, as suggested by Upton and Goddard. We have also applied the model to ordered overlayers of sulfur on the Ni(100) surface, and we provide theoretical energy-loss spectra for this case. Throughout the discussion an emphasis is placed on features in the energy-loss spectrum which lie below the maximum phonon frequency of the substrate.

I. INTRODUCTION

High-resolution electron-energy-loss spectroscopy has proved to be a powerful tool in the study of the vibrational modes of atoms and molecules adsorbed on metal surfaces. For simple geometries, the application of the selection rule[1] introduced some years ago for near specular losses controlled by the dipole mechanism, and also those that apply to dipole inactive modes,[2] enables one to identify the symmetry of the adsorption site from the loss spectrum.[3] It is gratifying to see excellent agreement between adatom vibration frequencies measured in the experiments, and theoretical models which contain no adjustable parameters,[4] with adatom-substrate force constants deduced from Upton and Goddard's *ab initio* calculations[5] of the interaction energy between an adatom and a rigid substrate. For hydrogen, oxygen, and sulfur on the Ni(111) and the Ni(100) surface the results are impressive.

Nearly all of the experiments confine attention to the study of high-frequency vibrational modes, with frequencies that lie well above the maximum phonon frequency of the substrate. Such vibrational frequencies are associated with modes that have vibrational motion highly localized to the near vicinity of the adsorbate. In the recent literature, experimental data has appeared in which loss spectra show clear features in the spectral region below the maximum frequency of the substrate.[6–8] Here, as discussed many years ago,[9] one expects to see lines in the energy-loss spectrum produced by surface phonons which lie in the gaps of the phonon dispersion curves of the bulk crystal, and in addition broad energy-loss bands of comparable integrated intensity produced by scattering from the continuous spectrum of bulk phonons with wave vector $\vec{Q}$ whose projection $\vec{Q}_{||}$ onto a plane parallel to the surface is selected by the scattering geometry.

The purpose of this paper is to present the results of a detailed theoretical study of a lattice-dynamical model of the $p(2\times2)$ and $c(2\times2)$ overlayer of oxygen on the Ni(100) surface. We constrain the parameters which enter the model by the requirement that it provides an adequate fit to the bulk phonon spectrum and also to the potential-energy curves calculated by Upton and Goddard,[5] for interaction of an oxygen atom with a rigid cluster of twenty Ni atoms arranged to mimic the semi-infinite Ni crystal with a (100) surface. The aim of the analysis is to make contact with the electron-energy-loss studies of these systems; here for both overlayers we have structure in the loss spectrum below the maximum phonon frequency of Ni (295 cm^{-1}). The spectra of Lehwald and Ibach are of particular interest because they are taken with extremely high resolution (3.7 meV or 30 cm^{-1}). In this study, as in the work of Andersson,[6] it is the near-specular dipole-active losses that are explored. From the scattering kinematics, the experiments thus explore the frequency spec-

trum of phonon-induced fluctuations in dipole moment perpendicular to the surface,[1] with wave vector $\vec{Q}_{||}$ parallel to the surface very close to the Γ point of the two-dimensional unit cell appropriate to the crystal surface with the adsorbate layer present.

Our aim is twofold. We wish to see to what extent a highly constrained lattice-dynamical model such as that described above fits the *frequency* spectrum of the surface vibrations. In addition, we explore a number of theoretically generated loss spectra which illustrate features of the lattice dynamics of surfaces not explored in previous studies, so far as we know. For example, an adsorbate lightly coupled to the surface will, if the substrate atoms are pinned rigidly in place, vibrate with eigenfrequency which lies below the maximum phonon frequency ω_M of the substrate. Then if the substrate atoms are allowed to move, the adsorbate mode no longer remains a vibrational mode localized to the surface, but rather becomes a resonance mode with finite lifetime (in the harmonic approximation) since the adsorbate may radiate phonons into the substrate. Low-frequency hindered rotations of adsorbed molecules should be described as resonance modes with this character, so it is of interest to explore the width of such features even within a model where the parameters are adjusted artificially. Thus, we wish to see how well the constrained model fits the data, and at the same time by adjusting parameters we can create a model system that may be used to explore some general questions in surface lattice dynamics.

A comparison between our calculated spectra and those obtained from electron-energy-loss experiments has led to some new results which we summarize briefly here. This will provide some justification for the various adatom geometries explored later in the paper. Upton and Goddard find two equilibrium positions, 0.88 and 0.55 Å, for an oxygen adatom at a hollow site of fourfold symmetry above a Ni_{20} cluster arranged to mimic a (100) crystal surface. We find excellent agreement between spectra calculated for a $p(2\times2)$ overlayer and the electron-energy-loss data for the adatom at 0.88 Å, and poor agreement between spectra calculated for a $c(2\times2)$ overlayer and electron-energy-loss spectra for either position. Upton and Goddard then consider binding of an oxygen above the fourfold-hollow site of a Ni_{20}^{+} cluster, for which they obtain an equilibrium distance of 0.26 Å (for a binding configuration similar to that which previously gave 0.55 Å). They argue this should mimic more closely the situation when there is a dense oxygen adlayer on the surface, such as occurs with a $c(2\times2)$ overlayer. In fact, we find excellent agreement between our calculated spectra and the experiment when this last equilibrium position is used.

We note that the $p(2\times2)$ overlayer of oxygen on Ni(100) has been examined by low-energy electron diffraction (LEED),[10] and comparison with theory shows the $p(2\times2)$ layer is 0.9 Å above the Ni(100) surface,[11] in good accord with the picture that results from the present study. However, the LEED data has been interpreted to suggest that the $c(2\times2)$ structure is also 0.9 Å above the surface; this is in disagreement with our conclusions. Recent photoemission data has also been interpreted by assuming that in the $c(2\times2)$ structure the oxygen lies very close to the Ni surface.[12]

This paper is organized as follows. In Sec. II we present a summary of a study we have carried out of the effective dipole moment seen by an electron in the vacuum *above* a metal surface when a substrate nucleus vibrates. Our conclusion is that as for an adatom placed above the surface,[1] only dynamic dipole moments normal to the surface lead to the strong "dipole lobe" seen in near-specular electron-energy-loss experiments. In our analysis of the spectrum, we find no evidence for scattering from parallel motions of the substrate atoms; this is discussed later in the paper. Section III describes construction of the basic lattice-dynamical model, then continues on to derive analytic expressions for certain lattice-dynamical Green's functions used ultimately in the discussion of electron-energy-loss spectra. Finally, in Secs. IV and V we discuss the calculations upon which the conclusions above are based, the effect of certain surface force-constant changes on these spectra, and also present theoretical calculations of the loss spectrum for other adatom-substrate combinations of the same basic geometry.

II. DIPOLE SCATTERING BY THE MOTION OF SUBSTRATE ATOMS

When one examines the angular distribution of low-energy electrons scattered inelastically from crystal surfaces by atomic vibrations there, one frequently observes a narrow cone of electrons centered about the specular direction. This near-specular lobe is a consequence of electric dipole scattering; as atoms on the surface vibrate, they

modulate the electric dipole moment of the surface. This produces fluctuating electric fields in the vacuum above the crystal surface, leading to the relatively intense small-angle scattering encountered frequently when long-ranged Coulomb fields are present.

The theory of this electric dipole scattering has been developed with primary attention directed to the scattering produced either by motion of the outermost atomic layer of atoms on clean semiconductor surfaces,[1] or that produced by adsorbates placed on the surface.[13] Here one encounters a selection rule, apparently consistent with a substantial body of experimental data,[3] which states that the only vibrational modes which are dipole active in the above sense are those which produce an oscillatory dipole moment normal to the crystal surface. To calculate the leading term in the electric field seen by the incoming electron when it is many lattice constants from the surface, one may use a model which places an oscillating dipole just outside the surface of a model dielectric; for a metal the low-frequency dielectric constant may be regarded as infinite in magnitude, to excellent approximation.

The experiments of primary interest to the present paper study scattering from modes where the atoms in the substrate participate importantly, as we shall see. If we picture the (metallic) substrate as a semi-infinite dielectric, with surface one-half interplanar spacing above the outermost layer of nuclei, then to consider dipole scattering produced by motion of the substrate nuclei, we are led to study the nature of the electric field seen by an electron above the crystal when a nucleus embedded within the substrate, rather than above it, is displaced. We consider this issue briefly in the present section within the framework of a simple model that is crude, but which we believe correctly depicts the basic physics.

We wish to consider, once again, the electric field felt by an electron above the surface, in response to a dipole placed in the substrate below the surface of a metal. The elementary dipole may be regarded as a pair of point charges of equal and opposite strength placed very close together. The superposition principle allows one to consider the field produced by a single point charge, and from this to synthesize the field generated by a dipole.

If a point charge is introduced deep into a metal, it will be surrounded by a cloud of screening charge with radius of the order of a Fermi-Thomas screening length,[14] so the electric field in the metal vanishes identically, except in the near vicinity of the external charge. Considerations of electrical neutrality require that a charge density with total integrated strength opposite that of the external charge be induced on the surface of the crystal. This surface charge density then produces the electric field seen by any charged particle outside the surface. Thus an essential feature of the theoretical analysis is proper inclusion of the surface charge density within a theory that conserves the total charge.

In a classic paper, Newns[15] has addressed the microscopic theory of the screening of an external charge introduced into a metallic film. Here, only the case of an external charge distribution with integrated charge of zero is considered explicitly, though prescriptions are stated for treating the general case. There is no explicit discussion of the effective surface charge density in this work and we feel that Newn's formalism will not lead to simple results with intuitive appeal. We have thus chosen to proceed by exploring a simpler but more schematic picture within which explicit analytic expressions may be obtained.

Let a charge of strength e^* be placed at position $\vec{r}'$ in the metal, with $\varphi_0(\vec{r})$ the potential outside and $\varphi_i(\vec{r})$ the potential inside. Quite clearly, outside the metal $\varphi_0(\vec{r})$ must satisfy Laplace's equation

$$\nabla^2\varphi_0(\vec{r})=0 \tag{2.1}$$

while inside we use a Fermi-Thomas model, with k_{FT} the inverse of the screening length:

$$(\nabla^2-k_{\mathrm{FT}}^2)\varphi_i(\vec{r})=-4\pi e^*\delta(\vec{r}-\vec{r}') \; . \tag{2.2}$$

The boundary conditions are that the electrostatic potential is continuous across the interface (this ensures continuity of tangential electric field $\vec{E}$), and that normal components of $\vec{E}$ are also continuous.

When we addressed the solution of the problem for a planar geometry, we found it difficult to achieve a solution which satisfies the requirement of charge neutrality. The surfaces of a film have infinite area, so a finite total surface charge is produced by an infinitesimally small charge density spread over the surface. The problem can be solved in closed form for a sphere with finite radius R, with the charge e^* placed a distance d from the surface. After one verifies that the condition of charge conservation is satisfied exactly for the finite sphere, one may take the mathematical limit $R\rightarrow\infty$ with d held finite to obtain the solution for a point charge placed near the surface of a semi-infinite metal.

We omit the details of the solution in the interest of brevity, and discuss only the results. Outside the sphere, the potential may be represented by the usual linear superposition of Legendre polynomial $P_l(\cos\theta)$ combined with the radial variation r^{-l-1}, while inside one combines the Legendre polynomials with modified Bessel functions of the third kind.

The results are summarized in Fig. 1, where we give a prescription for constructing the field seen by an electron far from the surface from an array of point charges combined with simple multiplicative factors. For a single point charge e^* placed below the surface [Fig. 1(a)], the potential seen above is equivalent to that produced by the pair of charges shown, multiplied by the screening factor $2\exp(-k_F d)/(k_F d)$. Thus, the charge e^* is completely screened to produce no field outside if $k_F d >> 1$.[16]

The results for a dipole placed below the surface and parallel to it follow directly from the superposition principle, as remarked above. The results are given in Fig. 1(b), where it is evident that the potential outside is *quadrupolar* in character. Thus, an oscillating dipole placed just below the surface and parallel to it will be "dipole inactive" in electron-energy-loss spectroscopy, just as is the case for a dipole placed on top of the substrate parallel, to the surface.

A dipole oriented normal to the surface generates an effective potential from an array of

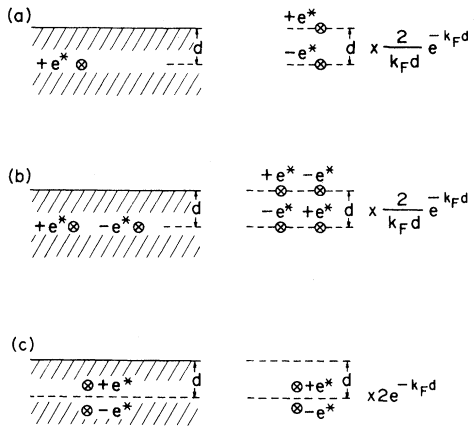

FIG. 1. The potential outside a metal surface produced by charges located below the surface. The potential is calculated within the Fermi-Thomas mode. The figure gives the rules for calculating the potential from (a) a single charge, (b) a point dipole oriented parallel to the surface, and (c) a point dipole oriented normal to the surface.

charges as shown in Fig 1(c). Note that as the dipole is allowed to approach the surface ($k_{FT}d << 1$), the electron outside the substrate sees a dipole with effective dipole moment twice as large as that produced by the same dipole moment placed in vacuum. This is precisely the same result as that obtained when the dipole is placed just above the surface.

Our conclusion is that for electron scattering produced by a subsurface species, the dipole selection rule operates in the same fashion as for an entity adsorbed on the surface. The vibrational motion must be such that an oscillating dipole moment normal to the surface is produced by the nuclear motion. Note that this does *not* require the atomic *displacements* to be normal to the surface. There are numerous examples of motions parallel to the surface which induce dynamic dipole moments normal to it.[3] We shall encounter an example in the present paper. The dynamic effective charge is in fact a tensor property of the crystal,[1] and this fact combined with the low symmetry of the surface environment allows for this possibility.

III. ORDERED OVERLAYERS AND LATTICE DYNAMICS OF THE fcc CRYSTAL WITH A (100) SURFACE

A. General remarks

To interpret the electron-energy-loss spectra that provide the primary motivation for this analysis, we require a description of the lattice dynamics of the crystal surface in a form suitable for contact with the data. This section is devoted to a discussion of the model we have used which is simple, but which has the virtue that few free parameters exist in it. We require it to reproduce the phonon spectrum of the bulk Ni crystal and be consistent with the *ab initio* calculations of Upton and Goddard.

The first step is to choose a two-dimensional unit cell for the structure. As one sees from Fig. 2(a), for the $c(2\times 2)$ overlayer one has one adatom and two substrate atoms per two-dimensional unit cell. For the $p(2\times 2)$ layer there is again one adatom and four substrate atoms per unit cell. In Fig. (2) we show our choice of unit cell for each structure. We illustrate this in Fig. 2(b). We denote the position of each atom through use of an index κ which specifies the site within the unit cell upon which a given atom resides, and a set of three integers that may be formed into a vector $\vec{l} = \vec{l}_{||}$

$+\hat{z}l_z$ which designates the unit cell within which the atom resides. Here l_z denotes the layer the atoms reside in, with $l_z=0$ the layer of adsorbed atoms and the crystal in the upper half-space. Then $\vec{l}_{||}$ gives the position of the unit cell within the plane. The equilibrium position of the atom is specified by the vector $\vec{R}_0(\vec{l}_{||}l_z\kappa)$. For the surface layer, since there is only one adsorbate atom per unit cell, the index κ may be dropped in the labeling of all quantities that enter. Thus, for example, the position of each adsorbate atom is specified by the vector $\vec{R}_0(\vec{l}_{||},0)$, with the adsorbate layer labeled by choosing $l_z=0$. Now for the fcc crystal with (100) surface, the various layers parallel to the surface are not identical, but one has a stacking sequence *ABABAB* . . . , where we form the *B* layers (even values of l_z) by shifting the *A* layer to the right [$\hat{x}$ direction in Fig. 2(a)] by the distance $a_0/2$. The distance a_0 is defined in Fig. 2(a). The labeling scheme in the *B* layers is thus derived from that in the *A* layers, shown explicitly in Fig. 2, by applying the above-mentioned shift.

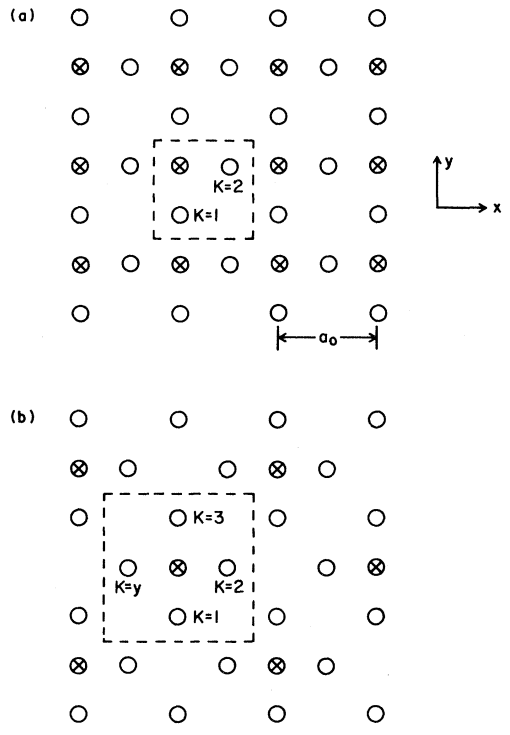

FIG. 2. The arrangement of atoms in the Ni(100) surface with (a) the $c(2\times2)$ and (b) the $p(2\times2)$ adsorbed layer present. The open circles are Ni atoms, the crossed circles are adsorbate atoms, and in each figure the two-dimensional unit cell of the structure is illustrated with dashed line.

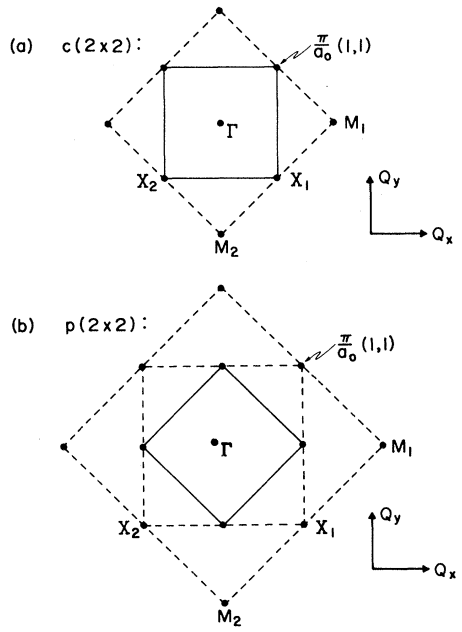

FIG. 3. The two-dimensional Brillouin zone for (a) the $c(2\times2)$ adsorbate-substrate combination, and (b) the $p(2\times2)$ adsorbate-substrate combination. In each case, the two-dimensional Brillouin zone of the clean surface is shown by dashed lines.

Finally, we require two-dimensional Brillouin zones for each of the two structures. These are illustrated in Fig. 3, together with the Brillouin zone of the clean (100) surface.

Throughout this section we shall assume the lattice dynamics of the system to be described by introducing an effective potential energy that depends only on the distance between the atoms. At a later point we shall introduce angle-bending interactions, which are formally three-body interactions. This may be done by modifying the equations presented here only slightly, as described later. Upon noting that all atoms within a given layer l_z have identical mass, the lattice-dynamical Hamiltonian in the harmonic approximation has the form

$$H=\frac{1}{2}\sum_{\vec{l}_{||}l_z\kappa}\frac{P^2(\vec{l}_{||}l_z\kappa)}{M(l_z\kappa)}+\frac{1}{2}\sum_{\vec{l}_{||}l_z\kappa;\,\vec{l}'_{||}l'_z\kappa'}\sum_{\alpha\beta}\Phi_{\alpha\beta}(\vec{l}_{||}l_z\kappa;\vec{l}'_{||}l'_z\kappa')\times u_\alpha(\vec{l}_{||}l_z\kappa)u_\beta(\vec{l}'_{||}l'_z\kappa'), \tag{3.1}$$

where $u_\alpha(\vec{l}_{||}l_z\kappa)$ is the αth Cartesian coordinate of the displacement of the atom away from equilibrium, and $\vec{P}(\vec{l}_{||}l_z\kappa)$ the associated momentum. If for the moment we replace the collection of symbols $(\vec{l}_{||}l_z\kappa)$ by simply i and j, then in the central force model the potential-energy term in Eq. (2.1) may also be arranged to read

$$V_2=\frac{1}{2}\sum_{ij}{}'\sum_{\alpha\beta}K_{\alpha\beta}(i,j)(u_{i\alpha}-u_{j\alpha})(u_{i\beta}-u_{j\beta}) , \tag{3.2}$$

where the prime instructs us to omit the terms with $i=j$, and where

$$K_{\alpha\beta}(i,j)=\frac{\varphi'_{ij}(d(ij))}{d(ij)}\delta_{\alpha\beta} + \left[\varphi''_{ij}(d(ij))-\frac{\varphi'(d(ij))}{d(ij)}\right] \times\hat{n}_\alpha(ij)\hat{n}_\beta(ij) . \tag{3.3}$$

In Eq. (3.3), $d(ij)$ is the distance between atom i and atom j at equilibrium, $\hat{n}(ij)$ a unit vector directed from i to j, and $\varphi'_{ij}(d(ij))$, $\varphi''_{ij}(d(ij))$ are the first and second derivatives of the two-body interaction evaluated at the equilibrium separation. A subscript ij appears on these quantities because the interaction potential between the adsorbate and substrate atoms differs from that of bulk substrate atoms, as does that between substrate atoms in and near the surface. The expressions in Eq. (3.1) and in (3.2) are linked by the relation

$$\Phi_{\alpha\beta}(ij)=\delta_{ij}\sum_{j'}K_{\alpha\beta}(ij')-(1-\delta_{ij})K_{\alpha\beta}(ij) . \tag{3.4}$$

In this section, we shall also confine our attention to the case where a given atom couples only to its nearest neighbors. Then if all nearest neighbors are equidistant from the atom in question, for the crystal to be in equilibrium one must have $\varphi'(d(ij))\equiv 0$. If the stated condition is violated or if we include interactions between more distant neighbors, then the equilibration condition is less simple. In fact, one expects the terms in $\varphi'(d(ij))$ in Eq. (2.3) to be small compared to those in $\varphi''(d(ij))$, so in what follows we shall invoke the commonly used approximation in lattice dynamics that ignores these contributions. Thus, for $K_{\alpha\beta}(ij)$ we shall use the approximation

$$K_{\alpha\beta}(ij)=\hat{n}_\alpha(ij)\hat{n}_\beta(ij)\varphi''_{ij}(d(ij)) . \tag{3.5}$$

Then for each pair of atoms, $K_{\alpha\beta}(ij)$ has magnitude controlled by only one parameter $\varphi''_{ij}(d(ij))$, and the form of this tensor depends on the orientation of the pair relative to the coordinate axes through $\hat{n}(ij)$.

For systems with two-dimensional periodicity such as the examples considered here, the equations of motion admit eigensolutions of the form

$$u_\alpha(\vec{l}_{||}l_z\kappa)=\frac{e_\alpha^{(s)}(\vec{Q}_{||};l_z\kappa)}{[M(l_z\kappa)]^{1/2}} \times\exp[i\vec{Q}_{||}\cdot\vec{R}_0(\vec{l}_{||}l_z\kappa)] , \tag{3.6}$$

where $\vec{Q}_{||}$ lies within the two-dimensional Brillouin zone illustrated in Fig. 3. Inclusion of the factor $M(l_z\kappa)$ is standard in lattice dynamics and leads to more convenient forms later, and the superscript s labels the particular eigenmode associated with the wave vector $\vec{Q}_{||}$ considered in Eq. (3.6). We may have surface phonons with displacement field localized near the surface, or solutions within the frequency bands alloted to those bulk phonons with dimensional wave vector $\vec{Q}$ whose projection onto the surface plane is given by $\vec{Q}_{||}$. The latter solutions describe bulk phonons that propagate up to and reflect off the surface. In general, these produce energy-loss bands in electron-energy-loss spectra with integrated intensity comparable to the peaks produced by scattering from surface phonons.[9] We shall see explicit examples of such features in the data taken by Lehwald and Ibach on the $c(2\times 2)$ layer of oxygen on the Ni(100) surface.

Rather than examine the equations of motion for the individual eigensolutions such as those in Eq. (3.6), we shall instead consider a set of Green's functions $U_{\alpha\beta}(l_z\kappa,l'_z\kappa';\vec{Q}_{||}z)$ defined by the statement

$$U_{\alpha\beta}(l_z\kappa,l'_z\kappa';\vec{Q}_{||}z)=\sum_s\frac{e_\alpha^{(s)}(\vec{Q}_{||};l_z\kappa)e_\beta^{(s)}(\vec{Q}_{||};l'_z\kappa')^*}{z^2-\omega_s^2(\vec{Q}_{||})} , \tag{3.7}$$

where the sum on s ranges over all eigenmodes associated with the wave vector $\vec{Q}_{||}$, $\omega_s(\vec{Q}_{||})$ is the frequency of the particular mode of interest, and z is a complex frequency. One may relate the spectral density formed

from such Green's functions directly to the energy-loss spectrum,[9] as we discuss below. A critical quantity is the spectral density function $\rho_{\alpha\beta}(l_z\kappa,l_z'\kappa';\vec{Q}_{||}\omega)$, defined as follows:

$$\rho_{\alpha\beta}(l_z\kappa,l_z'\kappa';\vec{Q}_{||}\omega)=i\frac{\omega}{\pi}[U_{\alpha\beta}(l_z\kappa,l_z'\kappa';\vec{Q}_{||},\omega+i\epsilon)-U_{\alpha\beta}(l_z\kappa,l_z'\kappa';\vec{Q}_{||},\omega-i\epsilon)]$$

$$\equiv\sum_s e_\alpha^{(s)}(\vec{Q}_{||};l_z\kappa)e_\beta^{(s)}(\vec{Q}_{||};l_z'\kappa')^*\delta(\omega-\omega_s(\vec{Q}_{||}))\ . \tag{3.8}$$

We can see how the spectral densities enter electron-energy-loss spectroscopy from the following argument. Suppose atom $(\vec{l}_{||}l_z\kappa)$ is displaced from its equilibrium and produces an effective dipole moment normal to the surface seen by an electron outside. We write this dipole moment $P_\perp(\vec{l}_{||}l_z\kappa)$ in the form

$$P_\perp(\vec{l}_{||}l_z\kappa)=\sum_\beta q_{\perp\beta}(l_z\kappa)u_\beta(\vec{l}_{||}l_z\kappa)\ , \tag{3.9}$$

where $q_{\perp\beta}(l_z\kappa)$ is a dipole-moment effective charge tensor similar to that introduced earlier,[1] and we allow the possibility that motions parallel to the surface generate a perpendicular dipole moment. Considerations of translational symmetry ensure that $q_{\perp\beta}(l_z\kappa)$ is independent of $\vec{l}_{||}$. The cross section for scattering from the particular mode $(\vec{Q}_{||}s)$ via the dipole mechanism is then proportional to[1]

$$|P_\perp^{(\mathrm{tot})}(\vec{Q}_{||},s)|^2=\sum_{\beta\beta' l_z\kappa,l_z'\kappa'}\frac{q_{\perp\beta}(l_z\kappa)q_{\perp\beta'}(l_z'\kappa')}{[M(l_z\kappa)M(l_z'\kappa')]^{1/2}}e_\beta^{(s)}(\vec{Q}_{||};l_z\kappa)e_{\beta'}^{(s)}(\vec{Q}_{||};l_z'\kappa')^*\ . \tag{3.10}$$

In an experiment, one generally does not detect scattering from a single eigenmode, but rather from all eigenmodes associated with the wave vector $\vec{Q}_{||}$ that lie in the frequency range between ω and $\omega+\Delta\omega$ (see below). The scattering efficiency per unit frequency is then proportional to the quantity

$$\frac{1}{\Delta\omega}\sum_s{}'|P_\perp^{(\mathrm{tot})}(\vec{Q}_{||},s)|^2=\sum_{\beta\beta' l_z\kappa,l_z'\kappa'}\frac{q_{\perp\beta}(l_z\kappa)q_{\perp\beta'}(l_z'\kappa')}{[M(l_z\kappa)M(l_z'\kappa')]^{1/2}}\rho_{\beta\beta'}(l_z\kappa,l_z'\kappa';\vec{Q}_{||}\omega)\ , \tag{3.11}$$

where on the left-hand side the sum on s includes all modes within the selected frequency interval $\Delta\omega$. Thus, given the spectral densities generated from Eq. (3.11) and a model of the manner in which nuclear motion generates an electric dipole moment, one can calculate the form of the energy-loss spectrum

We conclude this section with a brief summary of the scattering kinematics. If an electron of energy E_I strikes the surface to create a phonon $(\vec{Q}_{||}s)$ and an electron with energy E_s, then quite clearly we must have

$$E_s=E_I-\hbar\omega_s(\vec{Q}_{||})\ . \tag{3.12}$$

Only wave-vector components parallel to the surface are conserved (to within a reciprocal lattice vector of the two-dimensionally periodic structure), so if $\vec{k}_{||}^{(s)}$ and $\vec{k}_{||}^{(I)}$ are the projections of the wave vector of the scattered and incident electron on the plane parallel to the surface, then we have

$$\vec{k}_{||}^{(s)}=\vec{k}_{||}^{(0)}-\vec{Q}_{||}+\vec{G}_{||}\ , \tag{3.13}$$

with $\vec{G}_{||}$ a two-dimensional reciprocal-lattice vector of the structure.

Throughout this paper we shall be concerned with studies of small-angle scatterings, where the electron energies lie within approximately one degree of the specular direction. Then $\vec{k}_{||}^{(s)}-\vec{k}_{||}^{(0)}$ is very much smaller than the length of the first nonzero reciprocal-lattice vector. We may set $\vec{G}_{||}=0$, and also $\vec{Q}_{||}$ is very close to zero on the scale set by the distance to the first Brillouin-zone boundary. Hence, to excellent approximation we need only the spectral densities associated with the point $\vec{Q}_{||}\equiv 0$ for both Brillouin zones illustrated in Fig. 2. For our models of the $c(2\times2)$ and $p(2\times2)$ overlayers on the (100) surface of an fcc crystal, and at the point $\vec{Q}_{||}=0$ of the Brillouin zone appropriate to the crystal with ordered overlayer present, we are able to solve for expressions for the relevant spectral densities by analytic method. We shall also use the continued fraction method[17] to extract information on features of the lattice dynamics away from the origin in the Brillouin zone. We shall see, for example, that even in the absence of direct lateral interactions between the

adsorbate atoms, indirect interactions through the substrate lead to a very substantial amount of dispersion in the surface phonon dispersion curves for oxygen and sulfur on the Ni surface. We first summarize the calculations based on analytic formulas, then we turn to a discussion of the application of the continued fraction method to the quasi-one-dimensional problems such as the present one. We find limitations of the method, as we apply it, not encountered in earlier studies of atomic motions of isolated adsorbate atoms on the surface,[4] and of atoms in the clean crystal surface.[16]

B. Lattice dynamics at the zone center for the $c(2\times2)$ overlayer; the case of nearest-neighbor central-force interactions

Quite generally, the Green's functions introduced in Eq. (3.7) may be found by generating the equations of motion satisfied by them. One begins by constructing the Fourier-transformed dynamical matrix $d_{\alpha\beta}(\vec{Q}_{||};l_z\kappa,l_z'\kappa')$ defined by the statement

$$d_{\alpha\beta}(\vec{Q}_{||};l_z\kappa,l_z'\kappa')=\sum_{\vec{l}'_{||}}\frac{\Phi_{\alpha\beta}(\vec{l}_{||}l_z\kappa;\vec{l}'_{||}l_z'\kappa')}{[M(l_z\kappa)M(l_z'\kappa')]^{1/2}}\exp\{i\vec{Q}_{||}\cdot[\vec{R}_0(\vec{l}_{||}l_z\kappa)-\vec{R}_0(\vec{l}'_{||}l_z'\kappa')]\}\ , \tag{3.14}$$

then noting that the Green's function satisfies

$$z^2U_{\alpha\beta}(l_z\kappa,l_z'\kappa';\vec{Q}_{||}z)-\sum_{l_z''\kappa''}\sum_{\gamma}d_{\alpha\gamma}(\vec{Q}_{||};l_z\kappa,l_z''\kappa'')U_{\gamma\beta}(l_z''\kappa'',l_z'\kappa';\vec{Q}_{||}z)=\delta_{\alpha\beta}\delta_{l_zl_z'}\delta_{\kappa\kappa'}\ . \tag{3.15}$$

It is a straightforward but tedious matter to work out the explicit form of the equations of motion for the semi-infinite fcc crystal with the $c(2\times2)$ overlayer. In the interest of brevity, we shall not quote the full form of these equations; instead, we examine one special subset of them. This will serve to illustrate the method we have used to obtain the results to be discussed in the next section.

Suppose we wish to find the Green's function $U_{zz}(0,0;\vec{Q}_{||}z)$ that may be used to form the spectral density associated with motion of the $c(2\times2)$ overlayer normal to the surface. Here for the oxygen overlayer the combination $l_z\kappa$ is replaced by 0; in what follows, we suppress reference to the combination $\vec{Q}_{||}z$. The equation of motion for $U_{zz}(0,0)$ then reads

$$(2k_{00}-z^2)U_{zz}(0,0)-k_{10}U_{zz}^{(+)}(1,0)=1\ , \tag{3.16}$$

where we define

$$U_{zz}^{(+)}(1,0)=U_{zz}(11,0)+U_{zz}(12,0)\ . \tag{3.17}$$

Also,

$$k_{00}=2\varphi_{10}''\sin^2(\theta_{01})/M_{\rm O}$$

and

$$k_{10}=2\varphi_{10}''\sin^2(\theta_{01})/(M_{\rm O}M_{\rm Ni})^{1/2}\ .$$

Here φ_{10}'' is the second derivative of the O-Ni pair potential evaluated at the equilibrium position, θ_{01} is the angle between the xy plane and a unit vector from a Ni atom in the outermost substrate atomic plane to its nearest-neighbor oxygen, and $M_{\rm O}$ and $M_{\rm Ni}$ are the mass of the oxygen and Ni atoms, respectively.

The next step is to form the equation of motion for the function $U_{zz}^{(+)}(1,0)$ that enters Eq. (3.16). This is given by

$$(2k_{12}+k_{10}'-z^2)U_{zz}^{(+)}(1,0)-2k_{12}U_{zz}^{(+)}(2,0)-2k_{10}U_{zz}(0,0)=0\ , \tag{3.18}$$

where $k_{10}'=2\varphi_{10}''\sin^2(\theta_{10})/M_{\rm Ni}$ and $k_{12}=2\varphi_{12}''\sin^2(\theta_{12})/M_{\rm Ni}$, with φ_{12}'' the second derivative of the pair potential between the Ni atoms in the outermost substrate layer ($l_z=1$) and the first subsurface layer of Ni atoms ($l_z=2$). The angle θ_{12} is defined similarly to θ_{01}; we allow for the influence of surface relaxation by allowing θ_{12} to differ from the bulk value of $\pi/4$ and for φ_{12}'' to assume a value different than the bulk Ni-Ni interaction φ_{22}''. If $k=\varphi_{22}''/M_{\rm Ni}$, then $U_{zz}^{(+)}(2,0)$ has the equation of motion

$$(2k_{12}+2k-z^2)U_{zz}^{(+)}(2,0)-2k_{12}U_{zz}^{(+)}(1,0)-2kU_{zz}^{(+)}(3,0)=0\ , \tag{3.19}$$

while for $l_z \geq 3$ we have

$$(4k - z^2)U_{zz}^{(+)}(l_z,0) - 2k[U_{zz}^{(+)}(l_z-1,0) + U_{zz}^{(+)}(l_z+1,0)] = 0 \quad (l_z \geq 3) . \tag{3.20}$$

The physical content of this set of equations is that vertical motion of the oxygen adlayer at $\vec{Q}_{||}=0$, i.e., rigid motion of the layer perpendicular to the surface, excites similar motion in the first substrate layer, and this disturbance propagates down into the bulk of the crystal. We shall see that for the $p(2\times 2)$ overlayer its vertical motion at $\vec{Q}_{||}=0$ excites a motion of more complex character in the substrate. Our next task is to solve the hierarchy of equations displayed in Eqs. (3.16)–(3.20). Before we do so, we note that to find the Green's functions $U_{zz}(l_z 1;0)$ and $U_{zz}(l_z 2;0)$ that describe each of the Ni atoms at the two sites in the two-dimensional unit cell, we require in addition to $U_{zz}^{(+)}(l_z;0)$ also the combination

$$U_{zz}^{(-)}(l_z;0) = U_{zz}(l_z 1;0) - U_{zz}(l_z 2;0) . \tag{3.21}$$

These functions satisfy the homogeneous set of equations

$$(2k_{12} + k'_{10} - z^2)U_{zz}^{(-)}(1;0) = 0 , \tag{3.22a}$$

$$(2k_{12} + k - z^2)U_{zz}^{(-)}(2;0) = 0 , \tag{3.22b}$$

$$(4k - z^2)U_{zz}^{(-)}(l_z;0) = 0 , \quad l_z \geq 3 . \tag{3.22c}$$

Since the functions $U_{zz}^{(-)}(l_z;0)$ satisfy homogeneous equations, they vanish identically. Rigid vertical oscillations of the oxygen adlayer excites the two Ni atoms $\kappa=1$ and $\kappa=2$ equally in *all* substrate layers, so $U_{zz}^{(-)}(l_z;0)$ vanishes as a consequence. This is a special feature of the nearest-neighbor lattice-dynamical model currently under study. Later in the paper we shall see that when next-nearest-neighbor interactions are added, the vertical motion of the oxygen adlayer couples to the function $U_{zz}^{(-)}(l_z;0)$ for even values of l_z. We believe next-nearest-neighbor coupling is in fact weak in the systems of interest, for reasons that will become clear later.

To solve the system of equations displayed in Eqs. (3.16)–(3.20), one proceeds as follows. For all values of $l_z \geq 3$, Eq. (3.20) is solved by any function proportional to $\exp(-\alpha l_z)$, where the attenuation constant α is found from

$$e^{2\alpha} - \left[2 - \frac{z^2}{2k}\right] e^{\alpha} + 1 = 0 , \tag{3.23}$$

and in order that the disturbance induced by the vibrating oxygen layer decay into the bulk, that root of Eq. (3.23) for which $\mathrm{Re}(\alpha) > 0$ is selected.

Suppose the complex variable z is allowed to approach the real axis of the ω plane, as is required in the calculation of the spectral densities [Eq. (3.8)]. The maximum substrate phonon frequency of the model is $\sqrt{8k}$, and if we write $z=\omega \pm i\epsilon$, the behavior of α in this limit depends on whether $\omega > \sqrt{8k}$. If $\omega > \sqrt{8k}$, then independent of the sign of ϵ, Eq. (3.23) has a solution $\alpha = i\pi + \chi$, with χ real given by

$$e^{\chi} = \frac{\omega^2}{4k}\left[1 - \frac{8k}{\omega^2}\right]^{1/2} + \left[\frac{\omega^2}{4k} - 1\right] . \tag{3.24}$$

Thus, for $\omega > \sqrt{8k}$ the disturbance induced by the adsorbate layer decays exponentially as one moves into the crystal, with amplitude that changes sign as one moves from one layer to the next (this comes from the factor of $i\pi$ in $\alpha = i\pi + \chi$). For $\omega < \sqrt{8k}$ in the limit $\epsilon \to 0$, the solution to Eq. (3.23) has the form $z = \pm i\theta$, with the sign the same as that in $z = \omega \pm i\epsilon$, where

$$\sin\theta(\omega) = \frac{\omega}{\sqrt{2k}}\left[1 - \frac{\omega^2}{8k}\right]^{1/2} . \tag{3.25}$$

Hence for $\omega < (8k)^{1/2}$, α is pure imaginary and the disturbance induced by the oxygen adlayer penetrates deeply into the bulk. The oxygen adlayer thus couples to the bulk phonons of the substrate.

Once α is chosen as outlined above, the hierarchy of equations, (3.16) through (3.20), is readily solved by the ansatz

$$U_{zz}(0,0) = n_0(\omega) , \tag{3.26a}$$

$$U_{zz}^{(+)}(1,0) = n_1(\omega) , \tag{3.26b}$$

$$U_{zz}^{(+)}(l_z,0) = n_2(\omega)\exp[-\alpha(\omega)(l_z-2)] , \tag{3.26c}$$

where a set of inhomogeneous algebraic equations may be generated for the coefficients $n_0(\omega)$, $n_1(\omega)$, and $n_2(\omega)$ from Eqs. (3.16), (3.18), and (3.19); we omit the details. In the course of presenting our results (Sec. IV) we shall require additional Green's functions not generated by the equations presented here. We omit detailed description of these, and of a generalization of Eqs. (3.16)–(3.20) readily solved in closed form, at the price of complexity. [This generalization generates $U_{zz}^{(+)}(l_z;l'_z\kappa')$ for general values of $(l'_z\kappa')$.]

C. Lattice dynamics at the zone center for the $p(2\times2)$ overlayer; the case of nearest-neighbor central force interactions

As in the preceding section we once again examine the equations of motion that generate the Green's function $U_{zz}(0,0)$ that describes the frequency spectrum of the vibrations of the oxygen adsorbate layer normal to the surface within the nearest-neighbor central-force model. The equation of motion for this function now becomes

$$(2k_{00}-z^2)U_{zz}(0,0)-\tfrac{1}{2}k_{10}U_{zz}^{(L)}(1,0) +\tfrac{1}{2}s_{10}U_{\|z}^{(B)}(1,0)=1 , \quad (3.27)$$

where the constants k_{00} and k_{10} are the same as those that appear in Eq. (3.16), and the Green's function $U_{zz}^{(L)}(1,0)$ enters because vertical motion of the oxygen adlayer excites vertical motion of the outermost substrate layer. Here $U_{zz}^{(L)}(1,0)$ is a Green's function formed by summing over the four atoms in the unit cell illustrated in Fig. 2(b). For general l_z,

$$U_{zz}^{(L)}(l_z,0)=U_{zz}(l_z1,0)+U_{zz}(l_z2,0) +U_{zz}(l_z3,0)+U_{zz}(l_z4,0) . \quad (3.28)$$

The term in $U_{\|z}^{(B)}(1,0)$ enters Eq. (3.27) because for the $p(2\times2)$ structure, vertical motion of the oxygen atom also excites a breathing motion, parallel to the surface, of the square of four Ni atoms to which it bonds. The constant

$$s_{10}=2\varphi_{10}''\sin\theta_{10}\cos\theta_{10}/(M_{\rm O}M_{\rm Ni})^{1/2}$$

and the "breathing mode" Green's function is

$$U_{\|z}^{(B)}(l_z,0)=U_{xz}(l_z2;0)-U_{xz}(l_z4;0) +U_{yz}(l_z3;0)-U_{yz}(l_z1;0) . \quad (3.29)$$

To proceed, we need to generate the equations of motion satisfied by the two new functions $U_{zz}^{(L)}(1,0)$ and $U_{\|z}^{(B)}(1,0)$. For $U_{zz}^{(L)}(1,0)$, we obtain an equation of motion that couples us into no new Green's functions:

$$(2k_{12}+\tfrac{1}{2}k_{00}'-z^2)U_{zz}^{(L)}(1,0)-2k_{12}U_{zz}^{(L)}(2,0) -\tfrac{1}{2}s_{00}U_{\|z}^{(B)}(1,0)-2k_{10}U_{zz}(0,0)=0 . \quad (3.30)$$

Here $s_{00}=2\varphi_{10}''\sin(\theta_{01})\cos(\theta_{01})/M_{\rm Ni}$ can allow for relaxation between the outermost layer and the layer just below it, as explained in the preceding section.

The equation of motion of the "breathing" Green's function $U_{\|z}^{(B)}(1,0)$ couples into a new degree of freedom of the substrate layer below. This we call a rocking degree of freedom $U_{zz}^{(R)}(l_z,0)$. Atoms at the sites $\kappa=1$ and $\kappa=3$ in the *even* numbered substrate layers are excited in a motion normal to the surface, with the motion of the atoms at $\kappa=1$ excited 180° out of phase with those at the sites $\kappa=3$. [Recall the earlier discussion in this section which summarized how the sites in the unit cells of even numbered substrate layers are related to those in the odd numbered layers, as illustrated in Fig. 2(b).] We define

$$U_{zz}^{(R)}(l_z,0)=U_{zz}(l_z1,0)-U_{zz}(l_z3,0) , \quad (3.31)$$

and the equation of motion of $U_{\|z}^{(B)}(1,0)$ then becomes

$$(4k_{11}+c_{12}+\tfrac{1}{2}c_{00}'-z^2)U_{\|z}^{(B)}(1,0) -\tfrac{1}{2}s_{00}U_{zz}^{(L)}(1,0)+2s_{10}U_{zz}(0,0) -2s_{12}U_{zz}^{(R)}(2,0)=0. \quad (3.32)$$

Here we encounter a new set of force constants. One has $k_{11}=\varphi_{11}''/M_{\rm Ni}$, with φ_{11}'' the second derivative of the pair potential between nearest-neighbor Ni atoms in the surface plane. Then $c_{12}=2\varphi_{12}''\cos^2(\theta_{12})/M_{\rm Ni}$, $c_{00}'=2\varphi_{10}''\cos^2(\theta_{10})/M_{\rm Ni}$, and $s_{12}=2\varphi_{12}''\sin(\theta_{12})\cos(\theta_{12})/M_{\rm Ni}$. The various coupling constants are written in a form that allows for changes in the intralayer interaction strengths, interlayer coupling strengths, and derivations of certain bond angles from the bulk values caused by, for example, interlayer relaxation.

The new Green's function $U_{zz}^{(R)}(l_z,0)$ introduced in Eq. (3.31) obeys an equation that introduces no new mathematical structures:

$$(2k+2k_{12}-z^2)U_{zz}^{(R)}(2,0)-s_{12}U_{\|z}^{(B)}(1,0) -kU_{\|z}^{(B)}(3,0)=0 , \quad (3.33)$$

for l_z even and greater than 2, the equation obeyed by $U_{zz}^{(R)}(l_z,0)$ identical to Eq. (3.33), but with k_{12} and s_{12} set equal to k. For $l_z\geq3$ the two remaining functions obey the set of equations

$$(4k-z^2)U_{zz}^{(L)}(l_z,0)-2kU_{zz}^{(L)}(l_z-1,0) -2kU_{zz}^{(L)}(l_z+1,0)=0 , \quad (3.34)$$

while a slightly modified form applied to $l_z=2$. Also

$$(6k-z^2)U_{\|z}^{(B)}(l_z,0)+2kU_{zz}^{(R)}(l_z-1,0) -2kU_{zz}^{(R)}(l_z+1,0)=0 . \quad (3.35)$$

We see that except near the surface of the material, the function $U_{zz}^{(L)}$ is decoupled from both $U_{||z}^{(B)}(l_z,0)$ and also $U_{zz}^{(R)}(l_z,0)$. Then for our purposes, Eq. (3.33) (with $s_{12}=k_{12}=k$) forms a hierarchy for which the "breathing" Green's function in odd numbered layers drives the "rocking" Green's function in the even numbered layers. Thus, Eq. (3.34), combined with Eqs. (3.33) and (3.35) form two sets of "non-interacting" hierarchies in the bulk of the material which are mixed by the oxygen adlayer at the surface, along with force-constant changes. These equations may be solved by the appropriate extension of the method used in the preceding section. Each hierarchy is solved in the bulk by an exponential ansatz similar to that in Eq. (3.26c). In fact, the solution for $U_{zz}^{(L)}(l_z,0)$ has precisely the same form as that given in Eqs. (3.26), with α found from Eq. (3.23). Equation (3.33) in the regime $l_z \geq 4$, where we are to set $k_{12}=k$, $s_{12}=k$, combined with Eq. (3.35) are solved by writing

$$U_{||z}^{(B)}(l_z,0)=n_{||}(\omega)\exp(-\alpha' l_z) \quad (l_z \geq 3; l_z \text{ odd}) \tag{3.36a}$$

and

$$U_{zz}^{(R)}(l_z,0)=n_R(\omega)\exp(-\alpha' l_z) \quad (l_z \geq 4, l_z \text{ even}) . \tag{3.36b}$$

One finds α' by solving

$$\sinh(2\alpha')=\frac{(6k-z^2)(z^2-4k)}{4k^2} , \tag{3.37}$$

while the ratio $n_{||}(\omega)/n_R(\omega)$ is given by

$$\frac{n_{||}(\omega)}{n_R(\omega)}=\frac{(4k-z^2)}{2k} . \tag{3.38}$$

Hence, solutions of the pair of Green's-function hierarchies in the bulk lead to a solution with two free parameters, the analog of $n_2(\omega)$ in Eq. (3.26c) which we call here $n_L(\omega)$, and either $n_{||}(\omega)$ or $n_R(\omega)$. Modifications of the basic bulk solutions for the various functions may be introduced by generalizing Eqs. (3.26) in the appropriate manner, and from the inhomogeneous set of equations near the surface the unknowns may be found.

Once again, we omit the details which are of little general interest. The equations displayed above and the associated discussion allow one to appreciate the nature of the substrate motion excited by vertical oscillation of the adsorbate layer. For the $p(2\times2)$ overlayer, the picture is considerably more complex than for the $c(2\times2)$ case, but it remains possible to solve the problem by analytic methods in which the last step involves the inversion of a small matrix that we have done with a computer program.

IV. RESULTS OF THE GREEN'S FUNCTION ANALYSIS

This section is devoted to the results of calculations of the electron-energy-loss spectrum generated by the Green's-function method described in the preceding section. We first consider in detail results for the $c(2\times2)$ and the $p(2\times2)$ overlayers of oxygen on the Ni(100) surface, with attention to a number of general points. Then we compare our results with the data reported by Lehwald and Ibach, and we conclude by presenting results calculated for other adsorbate-substrate combinations.

We begin with the simplest picture which ignores all force-constant changes near the surface. Thus we have only two parameters in the model. One is φ_{22}'', which controls the strength of the Ni-Ni interactions in the bulk. The maximum substrate phonon frequency in the bulk is $(8\varphi_{22}''/M_{\text{Ni}})^{1/2}$. For Ni, this is 295 cm^{-1}, so we have $\varphi_{22}''=3.79\times10^4$ dyne cm^{-1}. The nearest-neighbor central-force model provides quite a good fit to the Ni phonon spectrum, and there is no evidence for appreciable surface relaxation. Thus we believe this simple model provides an adequate picture of the lattice dynamics of the substrate. The one remaining parameter describes the strength of the interaction between an adsorbed oxygen atom and each of its four nearest Ni neighbors. We need to know the value of the parameter φ_{10}'' and also the angle θ_{10} introduced in Sec. III to find the entries in the dynamical matrix from this coupling. If $R_\perp$ is the distance of the oxygen atom above the Ni surface plane and a_0 the distance between nearest-neighbor Ni atoms, then $\sin(\theta_{10})=\sqrt{2}R_\perp/a_0$.

We find φ_{10}'' from the potential-energy curves calculated by Upton and Goddard, as follows. These authors calculate the interaction energy as a function of distance, as an oxygen atom is moved toward the fourfold hollow site, along the perpendicular to the surface of a Ni_{20} cluster arranged to mimic the semi-infinite Ni crystal with (100) surface. As the oxygen is moved, the Ni atoms are held fixed in position. The curvature of their potential-energy curve about the minimum then

gives a vibrational frequency that would be that for perpendicular motion of the oxygen above the Ni surface when the substrate atoms are regarded as infinitely massive. In the notation of Sec. III this frequency is $\sqrt{2k_{00}}$, so when θ_{10} is known we may find φ''_{10}.

For an oxygen atom above an electrically neutral Ni_{20} cluster, they find an equilibrium position for the oxygen atom ($R_\perp$) at 0.88 Å above the surface, and for this position $(2k_{00})^{1/2}=371$ cm^{-1}. For oxygen above the Ni surface (and not for any other adsorbate considered in their analysis), they find a second equilibrium position at $R_\perp=0.55$ Å with lower binding energy than the most favored position $R_\perp=0.88$ Å. These authors argue that this calculation should adequately describe binding appropriate to the low-density $p(2\times2)$ structure, but for the more dense $c(2\times2)$ structure there will be appreciable charge transfer between the adsorbate layer and the substrate and a better model would be the binding of an oxygen atom to a Ni_{20}^+ cluster. Here they find an equilibrium position of $R_\perp=0.26$ Å, and $(2k_{00})^{1/2}=264.5$ cm^{-1}. In essence, the electronic configuration appropriate to the earlier $R_\perp=0.55$ Å minimum becomes favored, and the adsorbate layer is pulled in tighter to the surface, in their view. The calculations below explore the electron-energy-loss spectra for the oxygen adlayer placed at various distances from the surface, with choice of force constants dictated by the results of Upton and Goddard.

In Fig. 4 we show calculations of the spectral densities relevant to electron-energy-loss experiments, for the $c(2\times2)$ oxygen overlayer placed 0.26 Å above the Ni(100) surface. The two curves are constructed as follows. One is the spectral density associated with vibrations of the oxygen adlayer normal to the surface. This is formed from the function $U_{zz}(0,0)$ obtained in Sec. III B using the prescription in Eq. (3.8). We refer to this spectral density as $\rho_O^{(\perp)}(\omega)$. This is compared with a second spectral density $\rho_{O\text{-}Ni}^{(\perp)}(\omega)$ formed for the normal coordinate

$$Z_1=u_z(0)-\tfrac{1}{2}[u_z(1,1)+u_z(1,2)]\ ,$$

which describes the *relative* motion of the oxygen adlayer and the outermost Ni layer. The latter spectral density, called the dipole-moment density function in earlier work by Allan and Lopez,[18] describes the energy-loss spectrum if in Eq. (3.11) we assume that only atomic motions normal to the surface lead to dipole scattering, and take the dynamic dipole moment of each Ni atom in the surface equal to half that of the oxygen adatom with the opposite sign. The physical picture then is that as the surface vibrates, the dynamic dipole moment is produced by charge transfer only between the adsorbate layer and the outermost layer of the substrate. There is rather little difference between these two spectral densities, except at rather low frequencies where $\rho_{O\text{-}Ni}^{(\perp)}(\omega)$ falls to zero because the adsorbate layer and the outermost substrate layer move in phase with equal amplitude. It is not hard to show that as $\omega\to0$, $\rho_O^{(\perp)}(\omega)$ tends to a constant while on physical grounds $\rho_{O\text{-}Ni}^{(\perp)}(\omega)$ vanishes. In the frequency regime of interest to most of the calculations we shall present, we find no dramatic difference between the spectral density of the vibrations of the adsorbate layer normal to the surface, and that associated with a normal coordinate such as described above.

When the oxygen adlayer is very close to the surface, as assumed in Fig. 4, the restoring force for motion normal to the surface is not large. From the work of Upton and Goddard we have once again $(2k_{00})^{1/2}=265.4$ cm^{-1}, which lies *below* the maximum substrate phonon frequency of 295 cm^{-1}. In this situation, when the motion of the coupled adsorbate substrate system is considered, the adsorbate layer does not lead to the appearance of vibrational modes (surface phonons) *above* the maximum substrate phonon frequency. All the normal modes of the system lie below 295 cm^{-1}, and the electron-energy-loss spectrum assumes the form of a continuous *band* of losses which extends

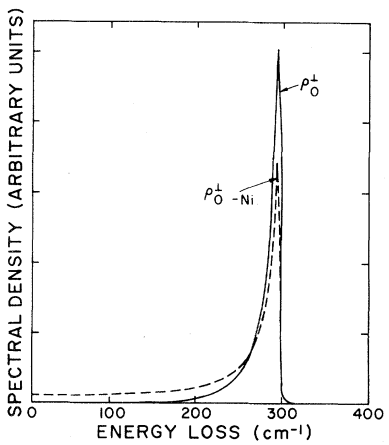

FIG. 4. The spectral density of fluctuations normal to the surface for the oxygen adlayer and for fluctuations in the distance between the adlayer and the outermost substrate layer. The calculations are for the $c(2\times2)$ overlayer, with parameters chosen as described in the text.

from zero frequency up to the maximum substrate phonon frequency. Very similar spectra were discussed some years ago for the clean (100) surface of an fcc crystal,[9] but one had to look at large scattering angles to see features such as those displayed in Fig 4. Here the adsorbate layer allows the phonons at the M point of the Brillouin zone of the *clean* (100) surface [see Fig. 3(a) of the present paper] to scatter electrons *near the specular* by the dipole mechanism. In the new Brillouin zone with adsorbate layer present, the M point is folded back to appear at Γ in the new zone.

In Fig. 5, again for the $c(2\times2)$ arrangement, we show a sequence of spectral densities calculated with rather different assumptions about the geometry. The curve labeled $R_\perp=0.88$ Å gives the energy-loss spectrum assumed to be described again by $\rho^{(\perp)}_{\text{O-Ni}}(\omega)$, for the case where the oxygen sits in the high position and k_{00} is chosen so $(2k_{00})^{1/2}=371$ cm^{-1}. The calculated energy-loss spectrum differs dramatically from the one shown in Fig. 4. There is a delta-function feature in the spectral density at 401 cm^{-1}. This is produced by the $\vec{Q}_{||}=0$ mode of a branch of surface phonons present when k_{00} is chosen this large. The shift from 371 cm^{-1} to 401 cm^{-1} has its origin in the motion of the substrate Ni atoms, which has the effect of shifting the "rigid substrate" frequency $(2k_{00})^{1/2}$ upward.[4] For $R_\perp=0.88$ Å, very little scattering is produced by the motions of the system in the frequency regime below 295 cm^{-1}. The contribution to $\rho^{(\perp)}_{\text{O-Ni}}(\omega)$ from this region can barely be discerned on the graph.

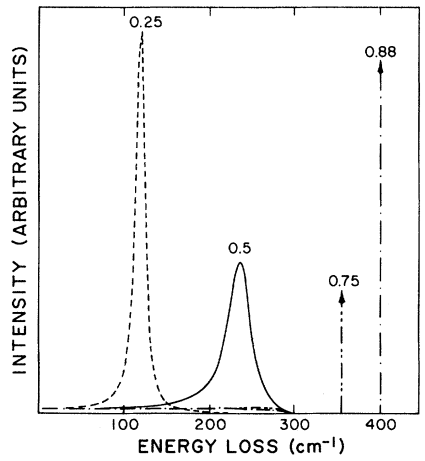

FIG. 5. For several values of the distance $R_\perp$ between the $c(2\times2)$ oxygen adlayer and the substrate, we show the frequency spectrum of the fluctuations in the distance between the adsorbed layer and the outermost layer of the substrate. See the text for a description of the choice of parameters.

To illustrate some general features of the lattice dynamics of the adsorbate layer, the remaining curves in Fig. 5 have been generated by keeping φ''_{10} fixed, then moving the oxygen layer downward, thus decreasing $(2k_{00})^{1/2}$ through action of the factor $\sin(\varphi_{10})$. When this is done for $R_\perp=0.75$ Å, we still have a surface phonon band above the substrate phonon frequency. This produces the delta-function feature indicated in the spectral density, and we still have little scattering within the bulk phonon bands. By the time $R_\perp=0.50$ Å, $(2k_{00})^{1/2}$ lies well below 295 cm^{-1} (it equals 232 cm^{-1}), and we now have a broad feature that looks as if it is produced by a mode with a rather short lifetime. This feature is in fact a resonance mode of the surface environment, qualitatively similar to those encountered in the lattice dynamics of imperfect crystals.[19] If the substrate atoms are held pinned in place while the adsorbate layer vibrates, we would have a surface phonon $\vec{Q}_{||}=0$, well below the maximum substrate phonon frequency at 232 cm^{-1}. Now if the adsorbate layer is excited and the substrate atoms are allowed to vibrate also, the energy associated with the adsorbate vibrational motion can be radiated into the crystal in the form of bulk phonons. The surface phonon thus acquires a finite lifetime in the harmonic approximation of lattice dynamics. The lifetime may be short, and no recognizable linelike feature may remain in the spectrum if coupling to the substrate is sufficiently strong and the density of bulk phonon modes at the relevant frequency is high. In essence, Fig. 4 provides an example of a situation where the coupling between the adsorbate layer and the substrate is so tight that no identifiable adsorbate resonance remains. In our example, as the oxygen layer is lowered further (again with φ''_{10} fixed), the $\vec{Q}_{||}=0$ resonance motion is shifted farther down in frequency and narrows to more closely resemble a real "mode" of the structure.

One expects to encounter such surface resonance modes commonly in the following situation. When a small molecule is adsorbed on a surface, there are high-frequency vibrations close in frequency and character to the internal modes of vibration appropriate to the gas phase. These generally lie well above the substrate phonon bands in frequency for the case where the substrate is a metal, though this may not always be so. There will be, in addition, low-frequency modes which owe their existence to the coupling between the molecule and the sub-

strate. These are often called "hindered rotations" and "hindered translations," a nomenclature that is rather imprecise because in general, a given mode will involve the combination of center-of-mass motion and rotation about the center of mass.[20] If, in a picture where the frequencies of the various modes are calculated first with the substrate atoms fixed in place, the influence of substrate motion on the modes is then explored, each mode may become a surface resonance mode such as those illustrated in Fig. 5 whenever its frequency lies below the maximum phonon frequency of the substrate. There is the distinct possibility that if the mode couples strongly to the substrate atoms or if its frequency lies in a regime where the density of substrate phonons is high, it may no longer appear in the energy-loss spectrum as a well-defined feature. Very shortly we shall encounter an example of just such a situation.

In Fig. 6(a) we show the energy-loss spectrum calculated for scattering from the $p(2\times2)$ overlayer of oxygen with $R_\perp=0.88$ Å. We have assumed once again that the relative motion perpendicular to the surface of the oxygen adlayer and the outermost Ni layer is responsible for setting up the dynamic dipole moment. It is important to note that here the "breathing" motion *parallel* to the surface of the square of Ni atoms just under each oxygen can generate a dynamic dipole moment *perpendicular* to the surface. In essence, on the right-hand side we should include the relevant off-diagonal elements $q_{\perp x}(1\kappa)$, $q_{\perp y}(1\kappa)$ in the dynamic effective-charge tensor so this feature is incorporated into the calculations. Since, as we see from Sec. III, the breathing coordinate is coupled to the vertical motion of the oxygen layer and that of the substrate for the $p(2\times2)$ structure, inclusion of this effect would influence the relative intensities of the features in Fig. 6, but no new structure would be introduced. It is hard to extract information on the relative intensities of the structures present in the data in a reliable fashion, so we have not included this feature in the calculations reported here.

We see three structures in Fig. 6(a). The first at 445 cm^{-1} is again the $\vec{Q}_{||}=0$ surface phonon associated with the oxygen layer, which for the $p(2\times2)$ is shifted up in frequency above the value 401 cm^{-1} found earlier for the $c(2\times2)$ structure.[21] The two remaining lines, one at 180 cm^{-1} and one at 245 cm^{-1}, are resonance modes very similar in character to those illustrated in Fig 5. They are distinctly asymmetric in shape, but very much

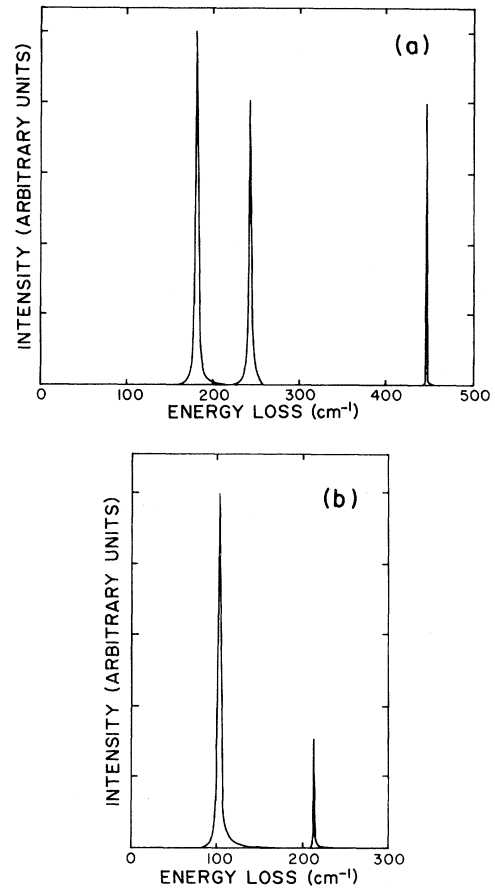

FIG. 6. For two choices of the distance between the oxygen adlayer and the surface (a) $R_\perp=0.88$ Å and (b) $R_\perp=0.26$ Å, we give the electron-energy-loss spectrum calculated as described in the text.

sharper to the point where they will be rather long-lived resonances of the surface.

It is clear that the feature at 245 cm^{-1} has its origin in the following. There is a surface phonon at the X point of the Brillouin zone of the clean (100) surface that was referred to some years ago as the S_6 mode.[22] This mode has displacements in the surface layer parallel to the surface, and is twofold degenerate since the eigenvectors at the X_1 and X_2 point illustrated in Fig. 3(a) are distinctly different. Upon forming the linear combination X_1+X_2 of these two eigenvectors, one obtains a pattern of displacement in which the square of Ni atoms under each oxygen breathe in phase. As we have seen, this excites a vertical oscillation of the oxygen adlayer which also excites similar motion in the outermost substrate layer, and the energy associated with the last mentioned motion is radiated off into the bulk. One of the two S_6 modes is thus

converted into a resonance mode by the presence of the $p(2\times2)$ overlayer and becomes dipole active at $\vec{Q}_{||}=0$ for reasons outlined above. The second S_6 surface mode, X_1-X_2, fails to excite the oxygen adlayer. We have been unable to relate the 180 cm^{-1} feature to any well defined feature of the lattice dynamics of the clean surface. The following calculation proves instructive, however. Suppose the second layer of Ni atoms and all interior substrate layers are regarded as rigidly fixed in position, and we consider the three degrees of freedom associated with coherent vertical oscillations of the oxygen adlayer, that of the outermost substrate layer, and in addition the breathing motion parallel to the surface of the outermost layer. This system has three normal modes at 446, 242, and 181 cm^{-1}, in rather good agreement with the three features in Fig. 6(a). Coupling to the remainder of the substrate then imparts a finite lifetime to the two low-frequency modes, since they may radiate their energy into the substrate in the form of bulk phonons.

In Fig. 6(b) we show a spectrum for scattering off the $p(2\times2)$ structure for φ''_{10} set equal to the value used to generate Fig. 6(a), but with $R_\perp$ decreased to 0.26 Å. We now see two modes, not three in the figure. These occur at 125 and 210 cm^{-1}. If we repeat the calculation discussed in the preceding paragraph where all layers but the adsorbate and first substrate layer are clamped in place, we find three modes 117, 156, and 247 cm^{-1}. The two lowest modes correspond to those in the figure. Our calculations indicate that the feature with origin in the S_6 mode never drops below the onset of the phonon continuum at the X point which begins at 210 cm^{-1} ($\sqrt{4k}$), and the two-layer calculation can never produce this "pinning effect" since it fails to include the full participation of the substrate. Upon examining our computed spectral density function, we do find a weak feature at 257 cm^{-1}. The structure is far too small to show on the scale of the graph in Fig. 6. This is an example of a situation where a surface mode lies inside the bulk phonon continuum, and fails to appear as a strong feature in the final spectral density. There are, in fact, three "modes" in the full calculation, with one rendered indistinct because of the effect of coupling to the substrate motions.

Another view of the three-peak structure is the following. A Ni_4O molecule in free space, with the four Ni atoms arranged on a square with the oxygen above its center, has three normal modes in which the oxygen moves in the vertical direction

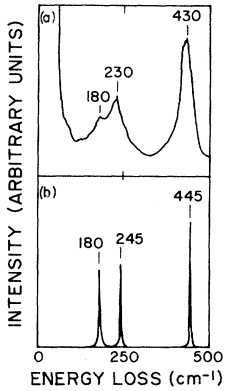

FIG. 7. We show here (a) the data of Lehwald and Ibach which explores near-specular energy loss of electrons scattered from the $p(2\times2)$ overlayer of oxygen on the Ni(100) surface, and (b) the energy-loss spectrum calculated with the model presented in the text with $R_\perp=0.88$ Å.

normal to the plane of the square. Two have finite frequency (435 and 130 cm^{-1} for our force constant model), and the third is the translational mode which has zero frequency for the free molecule. In essence, the calculations just described explore coherent vibrations of an ordered array of Ni_4O molecules bound to a rigid substrate. Here, by virtue of coupling to the substrate, the translation mode acquires a finite frequency, so we have the three finite-frequency modes. When all substrate atoms are allowed to vibrate, and not just those in the outermost layer, our calculations show that for the $p(2\times2)$ structure the basic three-mode picture survives, though the systematic trends (resonance mode character of structures below ω_M, "hanging up" of one mode at 210 cm^{-1}) reflect features of the lattice dynamics of the full substrate.

These calculations outline a number of basic features of the influence of an adsorbate layer on the lattice dynamics of crystal surfaces. We next turn to a comparison of our calculations and the data of Lehwald and Ibach.

In Fig. 7, the top figure presents the electron-energy-loss data taken by Lehwald and Ibach for the $p(2\times2)$ overlayer, and below this we show our theoretical spectrum calculated for the case where $R_\perp=0.88$ Å and φ_{10} is determined from setting 371 cm^{-1} as the oscillation frequency of an oxygen adatom against a rigid substrate. All three features in the theory show clearly in the data. There are no adjustable parameters in the theoretical model, thanks to Upton and Goddard, and we regard the

fit as quite remarkable. Later we shall explore the effect of various embellishments of the basic model. The fit between theory and experiment shows that their calculated potential-energy curves are very reliable, in our view.

The top entry in Fig. 8 shows the data for the $c(2\times2)$ structure. We assume the small and barely discernible feature at 440 cm^{-1} is not a loss intrinsic to this structure. One sees in the data a broad, asymmetric feature peaked just above the maximum Ni substrate frequency, with a tail that extends down into the phonon band. In Fig. 8(b) we show the spectrum also displayed in Fig. 4, which is calculated with the assumption that the oxygen is only a distance $R_\perp=0.26$ Å from the surface, as suggested by Upton and Goddard. A small adjustment in the parameters produces an improved comparison with the data. Figure 8(c) shows a calculation with φ''_{10} fixed with the same value used for Fig. 8(b), but with $R_\perp$ changed from 0.26 to 0.27 Å. Now a surface phonon is split off slightly from the Ni phonon bands, and the asymmetric tail is a bit broader. [The spectral density should be multiplied by $(1+n(\omega))$ before comparing with the data, where $n(\omega)$ is the Bose-Einstein function. This we have not done, and the Bose-Einstein factor would "lift" up the tail a bit more.] From Fig. 8 we see that by placing the $c(2\times2)$ layer very close to the Ni surface, we obtain good fit to the data. If, as suggested in the LEED literature, we were to place the $c(2\times2)$ layer 0.88 Å above the surface and use the force constants provided by Upton and Goddard, we would be lead to results in *qualitative* disagreement with the data. The relevant curve is that labeled $R_\perp=0.88$ Å in Fig. 5; we see a single line at 401 cm^{-1} and very little scattering below 300 cm^{-1}.

Our model may be criticized on the following grounds, however. While we obtain an excellent fit to the energy-loss data with the nearest-neighbor central-force model, for the $c(2\times2)$ structure a large value of φ''_{10} is required, simply because of the factor of $\sin^2(\theta_{10})$ which enters the constants k_{00}, k_{01}, and k'_{00} defined in Sec. III. The physical origin of this factor is clear; as the oxygen equilibrium position is lowered toward the plane defined by the four nearest-neighbor Ni atoms, φ''_{10} must be increased substantially for there to be a restoring force for perpendicular motions of the oxygen atom, if there are only nearest-neighbor central-force couplings. We have no restoring force at all from this source, for $\theta_{10}=0$ as one can easily see. Now for $R_\perp=0.26$ Å, the large value of φ''_{10} leads

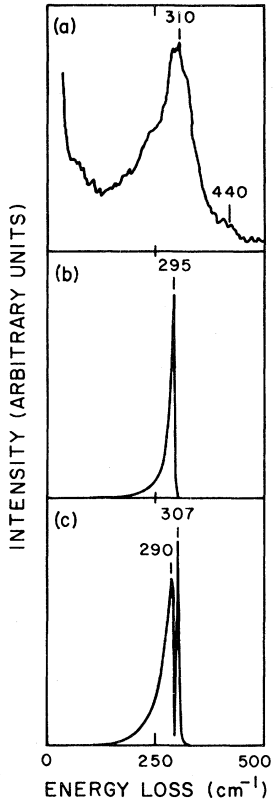

FIG. 8. (a) The data of Lehwald and Ibach, which explores near-specular energy loss of electrons scattered from the $c(2\times2)$ overlayer of oxygen on the Ni(100) surface, (b) the spectrum calculated with $R_\perp=0.26$ Å and φ''_{10} chosen as described in the text, and (c) the spectrum calculated with $R_\perp=0.27$ Å and φ''_{10} equal to the value used in (b).

to a very high-frequency adsorbate-induced surface phonon branch for oxygen motions *parallel* to the surface. At $\vec{Q}_{||}=0$, our model gives 1440 cm^{-1} for this frequency. We are unaware of any experimental data which contradicts this prediction, since such parallel motions of the oxygen atoms are not probed in the electron-energy-loss experiments to date, and we know of no molecules in which oxygen resides very near a planar configuration of four transition-metal ions. Nonetheless this frequency seems very high from an intuitive point of view, and one must inquire if the basic model may be modified without greatly affecting our calculated energy-loss spectra.

We have explored two possibilities, one of which appears quite reasonable. We first tried to add next-nearest-neighbor coupling of central-force character between the oxygen adatom and the Ni atom immediately below it in the second substrate

layer. Such coupling does not affect the frequency of vibration of the oxygen *parallel* to the surface in the harmonic approximation, but stiffens the response for motion perpendicular to it. One might expect such coupling to enter importantly in the description of the low-lying $c(2\times2)$ structure. By adding next-nearest-neighbor coupling, and decreasing the magnitude of φ''_{10}, we can lower the frequency for oxygen vibration parallel to the surface, while the effective spring constant for perpendicular motion is left unaffected. Figure 9 shows a calculation of $\rho_O^{(\perp)}(\omega)$ when the second-neighbor coupling constant assumes a value equal to one fifth of that associated with the nearest neighbor for $R_\perp=0.26$ (we mean that φ'' for the next-nearest-neighbor interaction is 0.2 times that for the nearest neighbor). We have used the continued-fraction method (see below) to obtain this result, and the small-amplitude oscillations are an artifact of the way in which the continued fraction was terminated. The prominent feature at 210 cm^{-1} in Fig. 9 is, however, absent in the data. The origin of this feature is as follows. In Sec. III we saw that the Green's function $U_{zz}^{(-)}(l_z;0)$ defined in Eq. (3.21) fails to couple to the oxygen vertical motion for the $c(2\times2)$ structure. The addition of next-nearest-neighbor interactions couples in this function. From Eq. (3.22b) we see that the second layer has a resonance at $\sqrt{4k}=210$ cm^{-1}, and hence the feature in the energy-loss spectrum displayed in Fig. 9. Our conclusion is that the presence of next-nearest-neighbor coupling of appreciable strength can be ruled out from the data, which provides no evidence of a structure at 210 cm^{-1}.

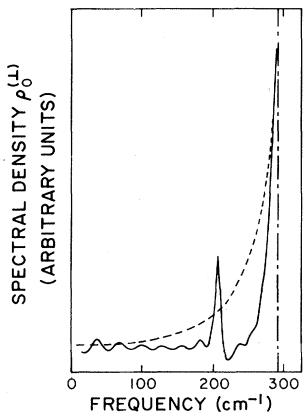

FIG. 9. The effects of second-neighbor interactions on the energy spectrum calculated for the $c(2\times2)$ structure. The dashed curve reproduces the spectral density in the absence of second-neighbor coupling, while the full curve includes second-neighbor coupling as described in the text.

It has been suggested by Ibach[23] that for a near-planar configuration of the oxygen Ni complex such as that we are led to for the $c(2\times2)$ structure, angle-bending interactions may influence the vibrational spectra importantly. Suppose we consider an oxygen atom placed a distance $R_\perp$ above a square arrangement of Ni atoms, and crudely mimic angle-bending interactions by adding to the potential energy a term of the form $\frac{1}{2}k_\theta(\theta-\theta_{10})^2$ for each O—Ni bond, where θ is the angle between a vector from the Ni atom directed toward the instantaneous position of the oxygen atom and the xy plane, while θ_{10} is the equilibrium position. A dimensionless measure of the relative importance of the angle-bending and nearest-neighbor central-force coupling is the ratio $\alpha=k_\theta/\varphi''_{10}a_0^2$. Ibach has argued that α cannot be terribly large,[23] possibly not much larger than 0.05. Now if we consider motions of the oxygen atom *perpendicular* to the plane of Ni atoms, if $u_\perp$ is the amplitude of the oxygen displacement, with nearest-neighbor central-force coupling included, the potential energy of the motion is

$$V_\perp=2\varphi''_{10}\sin^2(\theta_{10})\times[1+2\alpha\cos^2(\theta_{10})\cot^2(\theta_{10})]u_\perp^2\ , \tag{4.1}$$

while for parallel motion one has

$$V_{||}=\varphi''_{10}\cos^2(\theta_{10})[1+2\alpha\sin^2(\theta_{10})]u_{||}^2\ . \tag{4.2}$$

When θ_{10} is small, the angle-bending interaction enters the response for vertical motion importantly, but leaves the potential energy for perpendicular motion unaffected. For small value of θ_{10} and α, we can choose a modest value of φ''_{10} to obtain modest frequencies for parallel vibration, while there is an appreciable restoring force for vertical motion.

We have included the angle-bending contributions described above to the dynamical matrix, then recalculated the various spectral densities and frequencies, including the substrate motion fully. If we constrain φ''_{10} and α so Eq. (4.1) reproduces Upton and Goddard's potential-energy curve for $R_\perp=0.26$ Å, inclusion of angle-bending terms has no qualitative effect on the calculated electron-energy-loss spectrum. The column labeled $\omega_\perp$ in Table I gives the position of the peak in the energy-loss spectrum for various values of α; we see there is a systematic downward shift as α is in-

TABLE I. The influence of angle-bending interactions on the perpendicular and parallel motions of the $c(2\times2)$ layer of oxygen on Ni(100) for $R_\perp=0.26$ Å. For various values of α and for φ'_{10} and α constrained as defined in the text, the column labeled $\omega_\perp$ gives the peak in $\rho_O^{(1)}(\omega)$, which remains asymmetric as in Fig. 8(b). The column labeled $\omega_\parallel$ gives the frequency of the $\vec{Q}_\parallel=0$ optical phonon associated with motion parallel to the surface.

α	$\omega_\perp$ (cm^{-1})	$\omega_\parallel$ (cm^{-1})
0.00	295	1440
0.01	287	1037
0.02	282	853
0.03	280	742
0.04	278	667
0.05	278	609

creased, and one may appreciate from comparison of Figs. 8(b) and 8(c) that rather small changes in $R_\perp$ may compensate for this. Also shown in Table I is the frequency of the surface phonon at $\vec{Q}_\parallel\equiv0$ for motion parallel to the surface. As expected from Eqs. (4.1) and (4.2), this frequency decreases dramatically as α increases.

Our conclusion is that angle-bending contributions are likely important for the low-lying $c(2\times2)$ structure proposed here. To describe them, we need at least one more parameter in the model, and at the moment we have no data in hand which can be used to constrain the model. Motions of adsorbate layers parallel to the surface may be probed in electron-energy-loss studies which examine large-angle deflections.[24] Such experiments on the $c(2\times2)$ overlayer of oxygen on Ni(100) will provide crucial information on the lattice dynamics of this system.

Although in Fig. 7 we find very good agreement between the data of Lehwald and Ibach and our calculations, there appear minor discrepancies like the exact location of the peak frequencies and the relative energy-loss intensities. We have tried to obtain a better fit with the experimental data by varying the force constant for the coupling between Ni atoms in the first layer to those in the layer below. The result of our calculation for the $p(2\times2)$ overlayer is tabulated in Table II where f is given by the relation $k_{12}=fk$, with $k_{12}=2\varphi''_{12}\sin^2\theta''_{12}/M_{\rm Ni}$ and $k=\varphi''_{22}/M_{\rm Ni}$. The frequency $\omega_\perp$ gives us the positions of the peaks in the energy-loss spectrum, while in the next column the intensities of the loss peaks inside the phonon band are presented in arbitrary units. As obvious from the table we obtain best fit to the data when $f=0.7$, where not only the locations of the peaks are closer to that observed experimentally but also the relative intensities of the two peaks inside the phonon band. Such force-constant changes can easily be produced by relaxation of the outer layers by a few percent.[25]

TABLE II. Frequencies of features in the electron-energy-loss spectrum of the $p(2\times2)$ structure as a function of $f=k_{12}/k$.

f	$\omega_\perp$ (cm^{-1})	Intensity (arb. units)
1.5	186.67	1.233
	255.00	0.0016
	448.33	
1.3	185.00	1.181
	255.00	0.052
	448.33	
1.0	180.00	0.6683
	243.33	0.7317
	445.67	
0.8	176.67	0.8613
	235.00	1.421
	445.67	
0.7	175.00	1.000
	230.67	2.062
	445.67	
0.5	168.33	1.014
	226.67	1.242
	445.67	

We have also explored the possible influence of changes in the parameter k_{11}, which enters the near-specular energy-loss spectrum for only the $p(2\times2)$ structure. As k_{11} is chosen equal to $0.7k$, $1.0k$, and $1.3k$, respectively, the high-frequency 445-cm^{-1} mode shifts by only ±5 cm^{-1}. The low-frequency 180-cm^{-1} ($k_{11}=1.0k$) mode is most sensitive to changes in this parameter, moving from 155 cm^{-1} ($k_{11}=0.7k$) to 180 cm^{-1} ($k_{11}=1.0k$), then to 203 cm^{-1} ($k_{11}=1.3k$). Thus, a comparison with the data suggests k_{11} is not greatly changed from its bulk value, though for this conclusion to be strong, a systematic analysis of the data within a multiparameter space would be required. Our model is simple, and we do not believe such a sophisticated analysis is meaningful.

The discussion above has assumed that in the

near specular direction, the dipole selection rule operates so that dynamic dipole moments perpendicular to the surface are the only features probed in the experiment. We have calculated the loss spectrum that would be expected from our model if the dipole selection rule were violated, so motions parallel as well as normal to the surface scatter. We can do this by following the method outlined in Sec. III, but one calculates at $\vec{Q}_{||}=0$ the functions $U_{xx}(l_z\kappa,l_z'\kappa',\vec{Q}_{||},\omega)$ and $U_{yy}(l_z\kappa,l_z'\kappa;\vec{Q}_{||}\omega)$. Once again, for the nearest-neighbor central-force model with angle-bending contributions to the potential energy inserted as described earlier, it is possible to obtain these functions in closed form by analytic methods.

In Fig. 10, we show the frequency spectrum associated with relative parallel vibrations of the oxygen adlayer and outermost Ni layer for the model of the $c(2\times2)$ structure when it is 0.26 Å above the surface. The calculation has been carried out for the central-force model supplemented by angle-bending interaction with $\alpha=0.05$. The parameters are those chosen to generate Table II. We see the $\vec{Q}_{||}=0$ surface optical mode at 610 cm^{-1} and an asymmetric structure in the phonon bands near 200 cm^{-1}. In contrast to the case where the spectral densities were calculated for motions normal to the surface, the spectrum in Fig. 10 is very different from the data. We see no evidence in the data for scattering from dynamic dipole moments parallel to the surface.

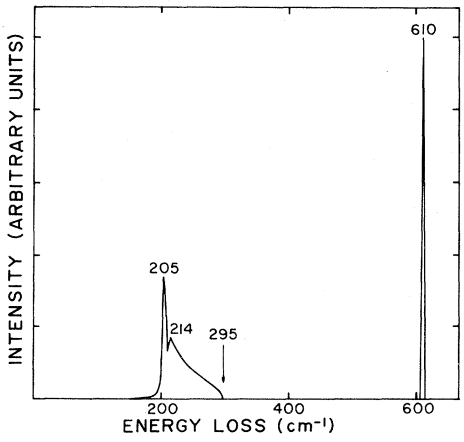

FIG. 10. The frequency for relative parallel motion of the adsorbate layer and outermost substrate layer for the $c(2\times2)$ oxygen layer placed 0.26 Å above the surface. The angle-bending parameter α has been chosen equal to 0.05; we have tried several values of α and found the shape of the feature below 295 cm^{-1} to be insensitive to this parameter.

We have also extended the calculation to the electron-energy-loss spectrum for $p(2\times2)$ and $c(2\times2)$ sulfur overlayers on the Ni(100) surface. Here again we have deduced the force constants and the perpendicular distance above the Ni surface where the sulfur atom sits in the hollow fourfold site, from the *ab initio* work of Upton and Goddard in the manner discussed earlier. Consequently, for both the overlayers we get the perpendicular distance ($R_\perp$) to be 1.24 Å, and the 393-cm^{-1} frequency for perpendicular motion leads to a value of 1.26×10^5 dyne cm^{-1} for φ_{10}''. In Fig. 11(a) we show the resulting spectrum for the energy-loss intensity for the $p(2\times2)$ coverage of sulfur on Ni(100) and in Fig. 11(b) we have the corresponding spectrum for the $c(2\times2)$ coverage. The $p(2\times2)$ overlayer of sulfur, with two peaks within the Ni phonon band (at 180 and 240 cm^{-1})

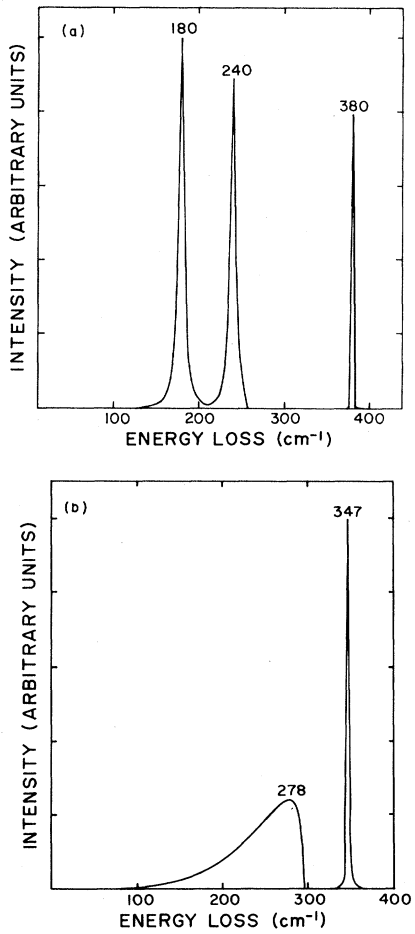

FIG. 11. The energy-loss spectrum for (a) the $p(2\times2)$ overlayer of sulfur on Ni(100) and (b) the $c(2\times2)$ overlayer of the same. The distance $R_\perp=1.24$ Å for both cases as described in the text.

and the localized sulfur mode at 380 cm^{-1}, as reminiscent of a similar oxygen overlayer on Ni(100) in Fig. 6(a). On the other hand, the $c(2\times2)$ overlayer of sulfur on Ni(100) [Fig. 11(b)] does not resemble that of oxygen on the same substrate (Fig. 4), because for sulfur we find much more scattering below the maximum phonon frequency of the Ni substrate. For the $c(2\times2)$ case of sulfur on Ni(100) we have the local mode at 347 cm^{-1} and an asymmetric peak at 278 cm^{-1} within the Ni phonon band. The only experimental data that we know of for sulfur on Ni(100) is that of Andersson[26] where he observes an energy-loss peak at 370 cm^{-1} for the $p(2\times2)$ overlayer and at 355 cm^{-1} for the $c(2\times2)$ one; the lower-frequency loss peak seems to be lost in the instrumental noise. We believe the observed peak to be the sulfur local mode which, as in our calculation, is downshifted for the $c(2\times2)$ overlayer as compared with the $p(2\times2)$ one. The agreement between theory and experiment for the case of sulfur suggests that in contrast to oxygen, the sulfur adlayer lies roughly the same distance above the surface for both structures. This is in accord with the view of Upton and Goddard who find only one equilibrium position for sulfur.

V. THE CONTINUED-FRACTION METHOD: THEORY AND DETAILS

A. General remarks

The results described in Sec. IV were all generated from analytic solutions to the equations of motion for the Green's functions. This approach becomes much more cumbersome when one moves away from $\vec{Q}_{||}=0$ in the two-dimensional Brillouin zone, though we have studies of an extension of it underway. This section is devoted to a description of a different method, the continued-fraction method, which also may be used to generate spectral density functions once the dynamical matrix is known.

The application of the continued-fraction method to problems in surface lattice dynamics has been discussed by Black, Laks, and Mills[17] for a model of the W(100) surface, and Black[4] has subsequently applied it to analyze the clean Ni(111) surface and that with isolated adatoms on it. In both papers the focus was not on the partially Fourier-transformed Green's function defined in Eq. (3.7) of the present paper, but rather on a closely related form $U_{\alpha\beta}(\vec{l}\kappa,\vec{l}'\kappa';z)$ obtained by Fourier-transforming the former with respect to $\vec{Q}_{||}$:

$$U_{\alpha\beta}(\vec{l}\kappa,\vec{l}'\kappa';z)=\frac{1}{N_s}\sum_{\vec{Q}_{||}}\exp\{i\vec{Q}_{||}\cdot[\vec{R}_0(\vec{l}'_{||}\vec{l}'_z\kappa')]\}\times U_{\alpha\beta}(l_z\kappa,l'_z\kappa';\vec{Q}_{||}z)\ . \tag{5.1}$$

The Green's functions defined in Eq. (5.1) are useful for the study of the frequency spectrum of particular atoms near the surface, such as an isolated adatom, and also for the calculation of mean-square displacement. In this section we describe our attempts to use the continued-fraction method to calculate the Green's functions defined in Eq. (5.1) and the partially Fourier-transformed form in Eq. (3.7), in the presence of an ordered overlayer. In Ref. 17, the reader will find a summary of the method, along with references to earlier work in the field.

The continued-fraction method when applied, for example, to the calculation of $U_{\alpha\alpha}(\vec{l}\kappa\,\vec{l}\kappa;z)$ defined in Eq. (5.1), provides a method for calculating a set of coefficients (A_n,B_n) which appear in the expansion

$$U_{\alpha\alpha}(\vec{l}\kappa,\vec{l}\kappa;z)=\cfrac{\cfrac{1}{|B_2|^2}}{z^2-A_1-z^2-A_2-\cfrac{|B_3|^2}{z^2-\cdots}}\ . \tag{5.2}$$

The issue of whether or not the method is useful in a particular instance centers on whether the sequence of coefficients (A_n,B_n) converges to a recognizable limiting behavior for n sufficiently small, say $n\lesssim10$. If this occurs, one may truncate the calculation of these at finite n, then extrapolate the series to $n=\infty$ and sum the remainder by analytic methods. Once again, the procedure is described in Ref. 17, and for the W(100) surface and the Ni(111) surface with isolated adatoms present, we found the method fast and easy to use with excellent convergence properties.

However, when we attempted to calculate the Green's functions $U_{\alpha\alpha}(\vec{l}\kappa,\vec{l}\kappa;z)$ for the Ni(100) surface with a $c(2\times2)$ overlayer of oxygen, we encountered convergence difficulties. For roughly 1600 atoms in the basic cluster, we found that the sequence A_n,B_n was oscillatory and had gone through only about one cycle by the time the iteration sequence led to sampling all atoms in the basic cluster. The number of atoms that must be

included in the basic cluster rises rapidly with the maximum value of n included in the sequence, and it was clear that we could not obtain adequate convergence with the computer available to us (Sigma 7). We believe the problem has its origin in the fact that the basic 1600-atom cluster includes rather few oxygen atoms (roughly 125), so the influence of the oxygen adlayer is only crudely accounted for with a cluster of this size.

We have also explored the calculation of the Green's functions in Eq. (3.7) with the continued-fraction method. The technique is exactly the same as that described in Ref. 17 once again, except it is the Fourier-transformed dynamical matrix in Eq. (3.14) which enters as the basic entity about which the iteration scheme is developed. In Table III we show the sequence of coefficients (A_n,B_n) calculated for the Green's function $U_{zz}(00)$ examined by analytic methods in Sec. III. This is the function frequency spectrum of perpendicular vibrations of the oxygen adlayer for the $c(2\times2)$ structure. We also show the sequence that generates the spectral density for the parallel vibrations and also that for the clean surface. The calculation used to generate Table III places the oxygen adlayer 0.88 Å above the surface. The first column gives the sequence (A_n,B_n) for generating $U_{zz}(0,0)$, the Green's function at $\vec{Q}_{||}=0$. We see rapid convergence, so the Green's function and spectral density are easily calculated for this case. The behavior exhibited in this sequence is quite different from that found for the isolated adatom case explored earlier, since there, even with n as large as 10, full convergence of the sequence was not obtained, though the sequence was smoothly approaching an asymptotic value. We have constructed the spectral density for the oxygen adatom with the continued-fraction method and compared the result with that generated by the analytic technique to find excellent agreement.

The next two columns show the results of the sequence for the case where $\vec{Q}_{||}$ is chosen at the X point of the two-dimensional Brillouin zone for the $c(2\times2)$ structure [Fig. 3(a)]. Here we see that B_n converges rapidly to a unique value, but A_n oscillates between two asymptotic values. In such cases, with the sequence (A_n,B_n) appropriately truncated, at $n=n_M$ one may use analytic methods to sum the remaining terms if the B_n is everywhere replaced by its asymptotic value B_∞ for $n>n_M$ while in this region A_n is allowed to oscillate between the two asymptotic values. We then obtain a form for the Green's function as adequate as that provided by the analytic approach.

The information in columns five and six of Table III explores the spectral density for parallel motion of the oxygen layer at the Γ point of the zone. The value of A_n and B_n oscillate here, and the first impression is that they each converge to a *pair* of final values, such that as $n\rightarrow\infty$ it alternates between these two values. If one assumes this to be the case, and extends the sequence to $n=\infty$ by analytic methods, the spectral density in Fig. 12(a) is generated. The result differs dramatically from that provided by the analytic method. A more careful analysis of the sequence shows, in fact, that in this and similar cases the sequence is converging to a single value of both A_n and B_n (in

TABLE III. Examples of the sequence (A_n,B_n) for various Green's functions for the $c(2\times2)$ adlayer of oxygen on Ni(100). For these calculations we have taken $R_\perp=0.88$ Å.

Atom and motion wave vector	Oxygen, ⊥ motion Γ point		Oxygen, ⊥ motion X point		Oxygen, || motion X point		(Clean surface) Ni surf. atom, ⊥ motion Γ point	
n	A_n	B_n	A_n	B_n	A_n	B_n	A_n	B_n
1	4878	0	4878	0	9763	0	777	0
2	1445	1805	4617	3611	3840	5109	1555	550
3	1555	777	1555	550	1244	869	1296	952
4	1555	777	2332	550	1796	733	1814	733
5	·	·	1555	550	1364	767	1555	673
6	·	·	2332	550	1708	794	1399	869
7	·	·	·	·	1433	743	1710	762
8			·	·	1654	812	1555	710
9			·	·	1477	737	1444	840
10					1616	817	1666	769

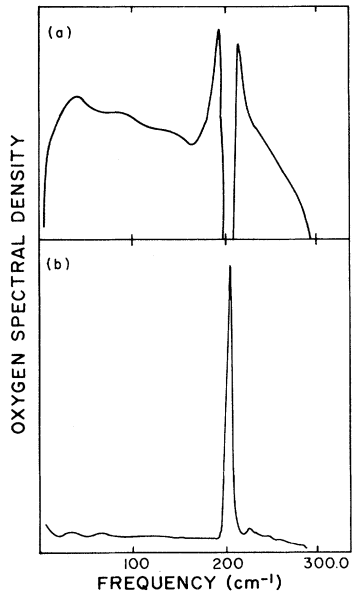

FIG. 12. The spectral densities for parallel motion of the oxygen at the Γ point of the two-dimensional Brillouin zone, calculated from the two different terminations described in the text. In (a), it is assumed (A_n,B_n) converges as each approaches a sequence that alternates between two values, while in (b) it is assumed that each converges to a unique asymptotic value.

this particular case 1554 and 777), but in an oscillatory fashion. If we use these values for all values of $n > 20$ to analytically sum the continued-fraction sequence, we obtain the results in Fig. 12(b). Note that the scales of Figs. 12(a) and 12(b) are different. The result in Fig. 12(b) comes close to matching that obtained from the analytic approach. It is not possible to extend the numerical computation beyond $n=20$ by the computational resources at our disposal. In fact, even with use of double precision it is difficult to carry the calculation beyond $n=10$ or 15 and still maintain sufficient accuracy. More terms are needed, in fact, to pin down the convergence properties unambiguously. We find this sort of difficulty occurs whenever there is a sharp feature, such as the resonance mode illustrated in Fig. 12(b), inside the bulk phonon band. The slow convergence of oscillatory character seems always to be present in the sequence (A_n,B_n) in such a situation.

The last two columns in Table III show the sequence of coefficients (A_n,B_n) for forming the spectral density at $\vec{Q}_{||}=0$, for motion of a Ni atom in the clean crystal surface in the direction perpendicular to the surface. Here there is again evidence of slow oscillatory convergence.

For values of $\vec{Q}_{||}$ at other general points in the surface Brillouin zone for the clean surface and also with the overlayer present, the behavior of the sequence (A_n,B_n) becomes more complex than that indicated in Table III, unfortunately.

At this point, we can make some overall comments on the strengths and the weaknesses of the continued-fraction method applied to surfaces with a periodic overlayer. Its chief strength lies in the fact that once the dynamical matrix $\underline{d}$ defined in Eq. (3.14) is known, the method can be applied to any atom or to any value of $\vec{Q}_{||}$, with no increase in computational labor required over that necessary for the points of high symmetry in the two-dimensional Brillouin zone. In addition, there is no great labor involved in adding second- and third-neighbor interactions or angle-bending contributions to the lattice potential energy; one merely makes the appropriate changes in $\underline{d}$ and the remainder of the calculation goes through unaltered.

However, when there are sharp resonances below the maximum phonon frequency of the crystal, we find it difficult to carry out the calculation of the sequence (A_n,B_n) sufficiently far and with sufficient accuracy for the convergence properties to become clear. One must then terminate the sequence of numerical calculations at some $n=n_M$, and for $n>n_M$ use possibly artificial values for A_n and B_n. The procedure becomes tedious and possibly unreliable; each Green's function must be examined individually and the appropriate procedure tailored to it. The method loses some of its attractiveness for the class of problems addressed in this paper, though we remind the reader that it has worked most impressively in our earlier studies.

When we studied vibrational modes which lie *above* the bulk phonon bands—most particularly the high-frequency surface optical phonons induced by an adsorbate layer, no matter how complicated the behavior of the sequence (A_n,B_n), we found three-figure convergence insensitive to the method of terminating the continued-fraction sequence. We next present results of calculations of the surface phonon dispersion curves for the structures of interest to us.

B. Dispersion of the adsorbate-induced surface phonon bands

In Sec. IV, for a number of situations examined in the spectral densities at $\vec{Q}_{||}=0$ we found surface phonon features at frequencies above the maximum

TABLE IV. Frequencies (cm^{-1}) of adatom vibrations perpendicular to the surface for various points in the two-dimensional Brillouin zone. The frequency ν_0 is that calculated in the limit of infinite substrate mass.

Perpendicular distance (Å)	ν_0	$p(2\times2)$ Γ point	$c(2\times2)$ Γ point	$c(2\times2)$ M point	$c(2\times2)$ X point
0.88	371	450	400	450	486
0.55	331	373	236	356	398
0.26	265		296	199	202

phonon frequency of the substrate. For example, for the $p(2\times2)$ oxygen overlayer on the Ni(100) surface, there is such a mode at 445 cm^{-1}, and this drops down to 400 cm^{-1} for the $c(2\times2)$ structure when $R_\perp=0.88$ Å. These surface phonons have frequencies that depend on the wave vector $\vec{Q}_{||}$ of the mode parallel to the surface. This is true even for the models such as those explored in Sec. III, which have no direct lateral coupling between the adsorbate atoms. In the absence of such coupling, there are indirect interactions between adsorbates through excitation of the substrate, and these indirect interactions are a source of a substantial amount of dispersion when the surface-mode branch lies not too far above the maximum phonon frequency of the substrate. This is discussed at some length elsewhere, where a method is developed to expand the dispersion relation in a power series with expansion parameter equal to the mass of the adsorbate atom divided by the substrate atomic mass.[3] Here we present exact results for the dispersion obtained from the continued-fraction method. Incidentally, the variation of the frequency of these modes with wave vector may be measured in off-specular electron-energy-loss experiments, as demonstrated in the very elegant work of Andersson and his colleagues.[26]

In Table IV we summarize our calculations of the dispersion in the surface-mode frequencies at selected points in the two-dimensional Brillouin zone for the dense $c(2\times2)$ structure, where we expect these effects to be largest. The first column gives the vibrational frequency for perpendicular motion of the oxygen adatom in the limit of infinite substrate mass for the three possible equilibrium positions discussed in the text. The second gives the frequencies at $\vec{Q}_{||}=0$ for the $p(2\times2)$ structure (discussed earlier), with the entry for $R_\perp=0.26$ Å omitted because the feature in question lies just below the maximum Ni phonon frequency and is barely visible in the spectral density. The last three columns give the frequencies at the Γ, M, and X points, respectively. It is intriguing that for $R_\perp=0.88$ Å, the surface-mode frequency increases as $\vec{Q}_{||}$ increases, while the opposite behavior is found for the low-lying $R_\perp=0.26$ Å position. In the latter case, all features in the spectral density lie below the maximum frequency of the Ni phonon bands, so we give the position of the peak in the principal prominent structure in each case. We hope that off-specular electron-energy-loss experiments may be able to explore the variation with $\vec{Q}_{||}$ of the features in the energy-loss spectrum.

ACKNOWLEDGMENTS

We are most grateful to T. Upton and W. A. Goddard for supplying us with their results in advance of publication, and for numerous stimulating discussions. Similarly, comments from and discussions with H. Ibach have been most useful. This research was supported by the U. S. Department of Energy through Contract No. DE-ATO 379-ER10432. One of us (J.E.B) wishes to acknowledge support from the National Science and Engineering Research Council of Canada.

[1]E. Evans and D. L. Mills, Phys. Rev. B 5, 4126 (1972).
[2]S. Y. Tong, C. H. Li, and D. L. Mills, Phys. Rev. Lett. 44, 407 (1980); Phys. Rev. B 24, 806 (1981).
[3]A general discussion of the selection rules within a group-theoretic framework and of the interpretation of electron-energy-loss spectra is given by H. Ibach and D. L. Mills, *Electron-Energy-Loss Spectroscopy and Surface Vibrations* (Academic, San Francisco, in press).
[4]J. E. Black, Surf. Sci. 100, 555 (1980), and in press.

[5]T. Upton and W. A. Goddard, Phys. Rev. Lett. 46, 1635 (1981); *Surface Science; Recent Progress and Perspectives* (Chemical Rubber, Cleveland, in press).
[6]S. Andersson, Surf. Sci. 79, 385 (1979).
[7]H. Ibach and D. Bruchmann, Phys. Rev. Lett. 44, 36 (1980).
[8]S. Lehwald and H. Ibach (unpublished).
[9]V. Roundy and D. L. Mills, Phys. Rev. B 5, 1347 (1972).
[10]J. E. Demuth and T. N. Rhodin, Surf. Sci. 45, 249 (1979).
[11]P. M. Marcus, J. E. Demuth, and D. W. Jepsen, Surf. Sci. 53, 501 (1975); M. Van Hove and S. Y. Tong, J. Vac. Sci. Technol. 12, 230 (1975).
[12]See the note added in proof in the paper by S. Kono, S. M. Goldberg, N. F. T. Hall, and C. S. Fadley, Phys. Rev. B 22, 6085 (1980).
[13]Review articles which include discussions of applications of the dipole scattering theory have been prepared by H. Froitzheim, in *Topics in Current Physics,* edited by H. Ibach (Springer, New York, 1976), Vol. 4; D. L. Mills, Prog. Surf. Sci. 8, 143 (1977). The principal results have been rederived by D. M. Newns, Phys. Lett. 60A, 461 (1977).
[14]Actually, of course, at large distances from the charge, one encounters the Friedel oscillations; it remains true that most of the net screening charge resides within a Fermi-Thomas screening length of the perturbation.
[15]D. M. Newns, Phys. Rev. B 1, 3304 (1970).
[16]Once again, the present model is not sufficiently complete to include the effect of Friedel oscillations, so the screening charge falls to zero monatomically as one moves away from the perturbation.
[17]J. E. Black, Bernardo Laks, and D. L. Mills, Phys. Rev. B 22, 1818 (1980).
[18]G. Allan and J. Lopez, Surf. Sci. 95, 214 (1980).
[19]See Chap. 8 of *Theory of Lattice Dynamics in the Harmonic Approximation,* edited by A. A. Maradudin, E. W. Montroll, G. H. Weiss, and I. P. Ipatova (Academic, New York, 1971).
[20]See Chap. 4 of Ref. 3.
[21]A reasonable account of these frequency shifts may be obtained by beginning with the "infinite substrate mass" picture, then expanding the frequencies in powers of the mass of the adsorbate divided by that of the substrate atom. This is discussed in Chaps. 4 and 5 of Ref. 3.
[22]R. E. Allen, G. P. Alldredge, and F. W. de Wette, Phys. Rev. B 4, 1661 (1971).
[23]H. Ibach (private communication).
[24]W. Ho, R. F. Willis, and E. W. Plummer, Phys. Rev. Lett. 40, 1463 (1978).
[25]D. Chang, thesis, University of California at Irvine (unpublished).
[26]S. Andersson and B. N. J. Persson, Phys. Rev. Lett. 45, 1421 (1980); B. N. J. Persson and R. Ryberg, Phys. Rev. B (in press).